Cell Reports
Medicine

Article

BRD9 inhibition overcomes oncolytic virus therapy resistance in glioblastoma

Graphical abstract

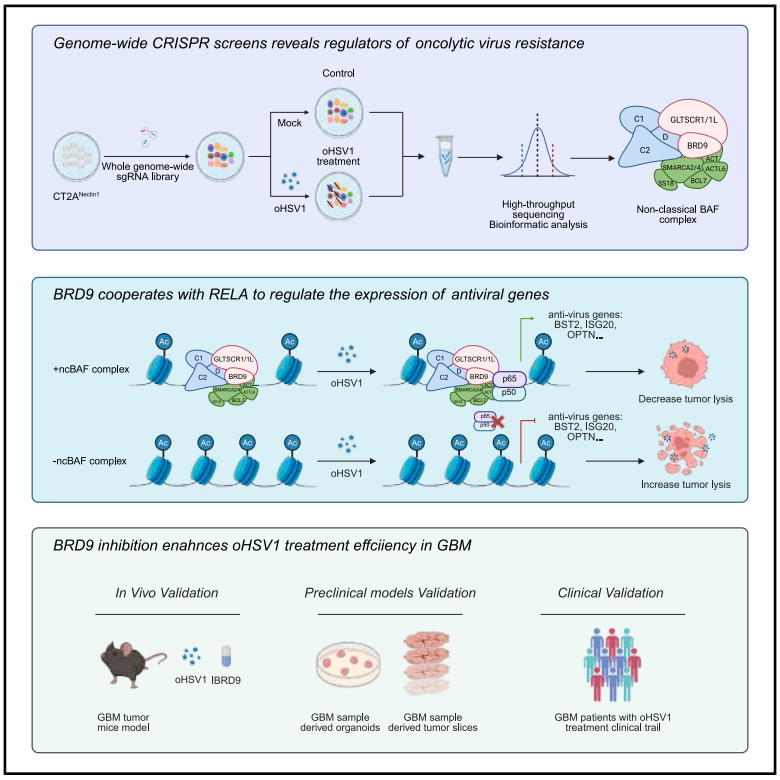

Highlights

- CRISPR screening identifies BRD9 as a key regulator of tumor resistance to oHSV1
- BRD9 inhibition enhances ICD and the antitumor activity of oHSV1 therapy
- BRD9 cooperates with RELA to regulate the expression of antiviral genes
- BRD9 is a potential biomarker for predicting clinical outcomes of oHSV1 therapy

Authors

Chen Guo, Zhilin Long, Peng Lin, ..., Yujia Cai, Chen Wang, Qi Xie

Correspondence

yujia.cai@sjtu.edu.cn (Y.C.), wc@ism.pumc.edu.cn (C.W.), xieqi@westlake.edu.cn (Q.X.)

In brief

Guo et al. perform a genome-wide CRISPR screen and identify BRD9 as a key regulator of tumor cell resistance to oncolytic virotherapy. BRD9 inhibition enhances ICD and promotes antitumor activity in multiple glioblastoma models, suggesting that BRD9 is a vital target for improving the efficacy of oncolytic virotherapy in GBM.

Guo et al., 2025, Cell Reports Medicine 6, 102258
August 19, 2025
https://doi.org/10.1016/j.xcrm.2025.102258

CellPress

Please cite this article in press as: Guo et al., BRD9 inhibition overcomes oncolytic virus therapy resistance in glioblastoma, Cell Reports Medicine (2025), https://doi.org/10.1016/j.xcrm.2025.102258

Cell Reports Medicine

CellPress
OPEN ACCESS

Article

BRD9 inhibition overcomes oncolytic virus therapy resistance in glioblastoma

Chen Guo,[1,2,3,4,10] Zhilin Long,[2,3,4,10] Peng Lin,[2,3,4,5,10] Yinan Shen,[6] Yiye Zhong,[7] Jingjing Qian,[2,3,4] Jichuan Yu,[2,3,4] Weixi Zhao,[2,3,4] Fuyi Liu,[8] Yiling Ma,[8] Jian Zheng,[8] Jiayao Yang,[2,3,4] Shuai Zhao,[2,3,4] Xiaojuan Ran,[2,3,4] Zhen Xia,[2,3,4] Congying Wu,[2,3,4] Yujia Cai,[7,9,*] Chen Wang,[5,*] and Qi Xie[2,3,4,11,*]

[1]College of Life Sciences, Zhejiang University, Hangzhou 310058, China
[2]Key Laboratory of Growth Regulation and Transformation Research of Zhejiang Province, School of Life Sciences, Westlake University, Hangzhou 310030, China
[3]Westlake Disease Modeling Laboratory, Westlake Laboratory of Life Sciences and Biomedicine, Hangzhou 310030, China
[4]School of Life Sciences, Westlake University, Hangzhou 310030, China
[5]National Key Laboratory of Immunity and Inflammation, Suzhou Institute of Systems Medicine, Chinese Academy of Medical Sciences & Peking Union Medical College, Suzhou 215123, China
[6]Department of Hepatobiliary and Pancreatic Surgery, The First Affiliated Hospital of Zhejiang University School of Medicine, Hangzhou 310003, China
[7]Key Laboratory of Systems Biomedicine (Ministry of Education), Shanghai Center for Systems Biomedicine, Shanghai Jiao Tong University, Shanghai 200240, China
[8]Department of Neurosurgery, The Second Affiliated Hospital of Zhejiang University School of Medicine, Hangzhou 310009, China
[9]State Key Laboratory of Medical Genomics, National Research Center for Translational Medicine at Shanghai, Ruijin Hospital Affiliated to Shanghai Jiao Tong University School of Medicine, Shanghai 200025, China
[10]These authors contributed equally
[11]Lead contact
*Correspondence: yujia.cai@sjtu.edu.cn (Y.C.), wc@ism.pumc.edu.cn (C.W.), xieqi@westlake.edu.cn (Q.X.)
https://doi.org/10.1016/j.xcrm.2025.102258

SUMMARY

Long-term survival of glioblastoma multiforme (GBM) remains challenging, spurring the development of novel therapies such as oncolytic virus therapy. While oncolytic virus shows promise in clinical trials, many patients do not respond to this therapy. Here, we perform a CRISPR screening and identify the non-canonical BRG1/BRM-associated factor (ncBAF) complex as a pivotal tumor-intrinsic factor for oncolytic virotherapy resistance. Knocking out the ncBAF-specific subunit bromodomain-containing protein 9 (BRD9) markedly augments the oncolytic efficacy of oncolytic herpes simplex virus type 1 (oHSV1) and enhances antitumor immunity. Mechanistically, BRD9 binds to RELA and potentiates the expression of downstream antiviral genes. Notably, the application of BRD9 inhibitor (IBRD9) significantly enhances the oncolytic activity of oHSV1 in various GBM models. Moreover, reduced BRD9 levels strongly correlate with improved outcomes in clinical trials of oHSV1. These findings suggest that BRD9 is an attractive target for overcoming the resistance to oHSV1 in glioblastoma treatment.

INTRODUCTION

The successful treatment of glioblastoma multiforme (GBM), one of the most lethal malignant tumors, remains greatly challenging.[1] Conventional interventions such as surgery, radiotherapy, and chemotherapy only achieve partial responses.[2] The highly immunosuppressive tumor microenvironment (TME) of GBM, marked by scant infiltration of antitumor lymphocytes, curtails the effectiveness of traditional immune checkpoint blockade therapies.[3–5]

Oncolytic viruses, which induce tumor cell lysis and modify the TME, can stimulate immune cells through viral exposure, potential tumor antigens, and tumor cell immunogenic cell death (ICD), making it a promising approach for GBM treatment.[6] Several early-phase clinical trials have demonstrated the therapeutic potential of oncolytic viruses for GBM.[7–9] However, a substantial number of patients remain unresponsive to this treatment, suggesting the existence of unidentified restriction factors that inhibit the optimal efficacy of oncolytic virus therapy in GBM.[5,8–10]

Here, through pooled whole-genome-wide CRISPR-Cas9 knockout screening, we identified the non-canonical BAF (ncBAF) complex as a crucial tumor-intrinsic factor that determines resistance to oncolytic viruses. Genetic or pharmacological targeting of the ncBAF-specific subunit bromodomain-containing protein 9 (BRD9) enhanced oncolytic virus replication and antitumor effectiveness, demonstrating the therapeutic potential of a combination therapy composed of oncolytic viruses and BRD9 inhibitors.

Please cite this article in press as: Guo et al., BRD9 inhibition overcomes oncolytic virus therapy resistance in glioblastoma, Cell Reports Medicine (2025), https://doi.org/10.1016/j.xcrm.2025.102258

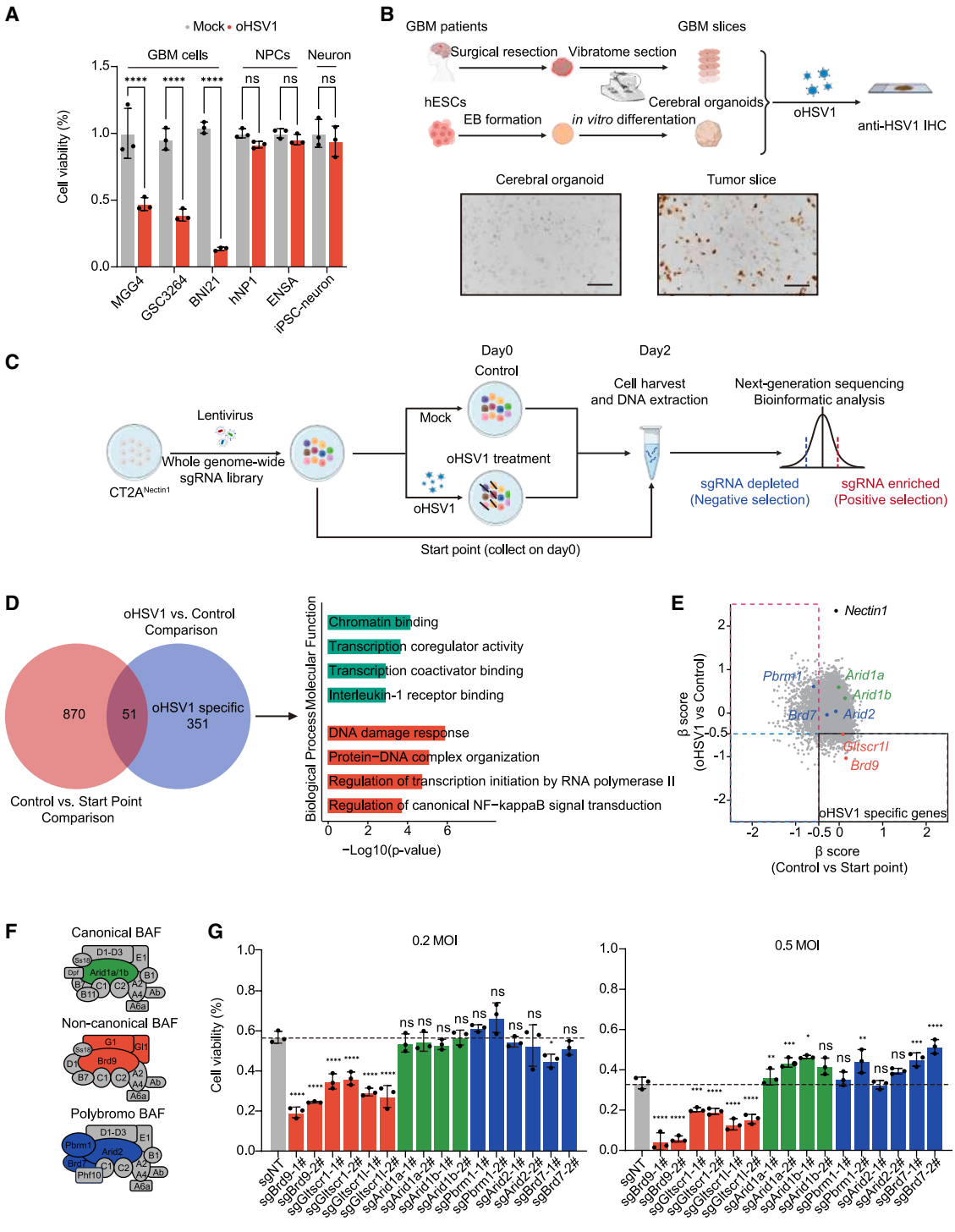

Figure 1. Genome-wide CRISPR screening reveals regulators of oncolytic virus resistance

(A) Cell viability of oHSV1-treated human glioblastoma cells (MGG4, GSC3264, and BNI21) and normal neural cells (hNP1, ENSA, and iPSC-derived neuron) (0.2 MOI, 24 hpi) (n = 3).

(B) Schematic illustration of cerebral organoid and patient-derived glioblastoma tumor section preparation with oHSV1 treatment. Analysis of oHSV1 replication in cerebral organoids and patient-derived glioblastoma tumor sections. After infection with oHSV1 (1×10^5 PFU, 24 hpi), the distribution of oHSV1 in the cerebral organoids and tumor sections was detected by anti-HSV1 immunohistochemistry. Scale bars, 100 μm.

(C) Schematic illustration of the CRISPR screening for oHSV1 treatment in CT2A^{Nectin1} cells.

(D) Venn diagram showing the intersection of essential genes from the oHSV1 treatment vs. control comparison and control vs. start point comparison (left). Gene Ontology analysis of the oHSV1-specific candidate genes (right).

(legend continued on next page)

Please cite this article in press as: Guo et al., BRD9 inhibition overcomes oncolytic virus therapy resistance in glioblastoma, Cell Reports Medicine (2025), https://doi.org/10.1016/j.xcrm.2025.102258

RESULTS

Genome-wide CRISPR screen reveals regulators of oncolytic virus resistance

To identify the genes that promote oncolytic virus therapy resistance, we selected oncolytic herpes simplex virus type 1 (oHSV1) for our study, as it is the most extensively used oncolytic virus in clinical trials for GBM.[11] The neurovirulence gene ICP34.5, typically deleted in early generations of engineered oncolytic viruses,[12,13] is also crucial for countering host cell antiviral responses and enhancing viral replication.[14] In our previous study, we engineered an oHSV1 by placing ICP34.5 under the control of miRNA-124, which is specifically active in neurons and often inactive in tumor cells, rather than completely removing it[15] (Figure S1A). We further assessed the effectiveness and safety of our oHSV1 in treating glioblastoma. Our oHSV1 selectively targeted and eradicated human glioblastoma cells (MGG4, GSC3264, and BNI21), with no detrimental impact on human normal neural progenitor cells (hNP1 and ENSA) or induced pluripotent stem cell (iPSC)-derived neurons (Figure 1A). We then utilized human embryonic stem cell-derived cerebral organoids and patient-derived glioblastoma slices to assess viral infection and replication (Figure 1B). Immunohistochemical anti-HSV1 staining revealed that viral replication was exclusively observed in the tumor sections (Figure 1B). Notably, unlike most human glioma cells, mouse glioma cells characteristically exhibit low expression of the herpes simplex virus type 1 (HSV1) entry receptor Nectin1, which impedes oHSV1 infection.[16] To address this issue and facilitate the study of oHSV1 therapy in immunocompetent mice, we overexpressed murine *Nectin1* gene in mouse glioma cell lines (CT2A and GL261) for subsequent investigations (Figure S1B). Furthermore, we confirmed the safety of our oncolytic virus *in vivo*, and immunohistochemical staining demonstrated that viral replication was restricted to tumor tissue (Figure S1C). Treatment with oHSV1 did not affect mouse survival and body weight nor did it alter the morphology of major organs (Figures S1D–S1F).

To identify genes that potentially promote resistance to oncolytic virus-mediated cytotoxicity, we performed a genome-wide CRISPR screen on mouse CT2A^{Nectin1} glioma cells. The lentivirus transduced tumor cells were treated with oHSV1 or control PBS (Figure 1C). The enrichment and deletion of single-guide RNAs (sgRNAs) between samples and hits identification were computed by Model-based Analysis of Genome-wide CRISPR-Cas9 Knockout (MAGeCK) software.[17] Also, we utilized the Bayesian Analysis of Gene Essentiality 2 (BAGEL2)[18,19] approach to confirm the quality of our CRISPR screening result (Figures S2A–S2F). Adopting the cutoff criteria of a β score of less than −0.5 and a *p* value of less than 0.05, we identified 402 potential genes that may confer resistance to oHSV1 infection (Figure 1D). To identify the specific genes that contribute to oHSV1 infection resistance, we excluded 51 genes that generally affect cellular proliferation in our screening data and then narrowed down the number of potential genes implicated in oHSV1-mediated cytotoxicity to 351 (Figure 1D). Gene Ontology analysis of these genes highlighted several significantly enriched molecular functions and biological processing, such as chromatin binding and protein-DNA complex organization (Figure 1D). Indeed, the positive selection of the HSV1 entry receptor *Nectin1*[16] in our screening data aligns with our expectations and further attests to the robustness and reliability of our screening approach (Figure 1E). Interestingly, we observed that unique subunits of the ncBAF complex, *Brd9*, and glioma tumor suppressor candidate region gene 1-like (*Gltscr1l*)[20] were enriched in oHSV1-specific gene selection (Figures 1E and 1F). In contrast, the unique subunits of the other two BAF complexes, canonical BAF (cBAF) complex and polybromo BAF complex, AT-rich interaction domain 1a (*Arid1a*), AT-rich interaction domain 1b (*Arid1b*), bromodomain-containing protein 7 (*Brd7*), polybromo 1 (*Pbrm1*), and AT-rich interaction domain 2 (*Arid2*),[20] were not enriched in this selection (Figures 1E and 1F). This finding suggested that the ncBAF complex may play an important role in suppressing oHSV1-mediated cytotoxicity and virus replication. We proceeded with the study by knocking out individual genes of the unique subunits of each BAF complex to examine the impact on oHSV1-mediated cytotoxicity in both mouse and human glioma models. Indeed, we found that knockout of the unique subunits of the ncBAF complex (*Brd9* and *Gltscr1l*) could enhance oHSV1-mediated cytotoxicity, whereas knockout of the unique subunits of the cBAF and polyBAF complexes did not significantly impact oHSV1-mediated cytotoxicity (Figures 1G and S2G). Thus, we identified that the ncBAF complex is an important promoter of oHSV1 resistance in glioblastoma cells.

BRD9 knockout enhances oHSV1-induced ICD and viral replication in glioblastoma cells

To investigate the role of the ncBAF complex in resistance to oHSV1 treatment, we focused on BRD9, a unique subunit of the ncBAF complex, which also has small-molecule inhibitors.[21,22] Knockout of BRD9 using two different sgRNAs did not impact cell proliferation in mouse or human glioblastoma

(E) Scatterplot for the β scores of each gene in the oHSV1 treatment group versus the control group and control group versus the start point group. The selected genes (921) in control vs. the start point comparison were gated in red frame. The selected genes (402) in oHSV1 treatment vs. control comparison were gated in blue frame. The oHSV1-specific genes (351) were gated in black frame. The positive selection *Nectin1* (black), canonical BAF subunits (green), non-canonical BAF subunits (red), and polybromo-associated BAF-specific subunits (blue) are highlighted.

(F) Diagram showing three different variants of switch/sucrose non-fermentable complex (SWI/SNF) complexes: canonical BAF (cBAF), noncanonical BAF (ncBAF), and polybromo-associated BAF (PBAF). cBAF-specific subunits (*Arid1a* and *Arid1b*) are colored green, ncBAF-specific subunits (*Brd9*, *Gltscr1*, and *Gltscr1l*) are colored red, and PBAF-specific subunits (*Arid2*, *Brd7*, and *Pbrm1*) are colored blue. Shared components among the complexes are colored gray (D1: *Smarcd1*; D2: *Smarcd2*; D3: *Smarcd3*; E1: *Smarce1*; B1: *Smarcb1*; A2: *Smacra2*; A4: *Smacra4*; Ab: *β-actin*; C1: *Smacrc1*; C2: *Smarcc2*; A6a: *Actl6a*; B7: *Bcl7*).

(G) Cell viability of oHSV1-treated CT2A^{Nectin1} cells (0.2 and 0.5 MOI, 24 hpi) transfected with sgRNA targeting the indicated SWI/SNF complex-specific subunits ($n = 3$).

Data represent mean ± SD. Unpaired two-tailed Student's t test (A), one-way ANOVA (G). The diagrams (B and C) were created using BioRender. $^{*}p < 0.05$, $^{**}p < 0.01$, $^{***}p < 0.001$, $^{****}p < 0.0001$; ns, not significant.

Please cite this article in press as: Guo et al., BRD9 inhibition overcomes oncolytic virus therapy resistance in glioblastoma, Cell Reports Medicine (2025), https://doi.org/10.1016/j.xcrm.2025.102258

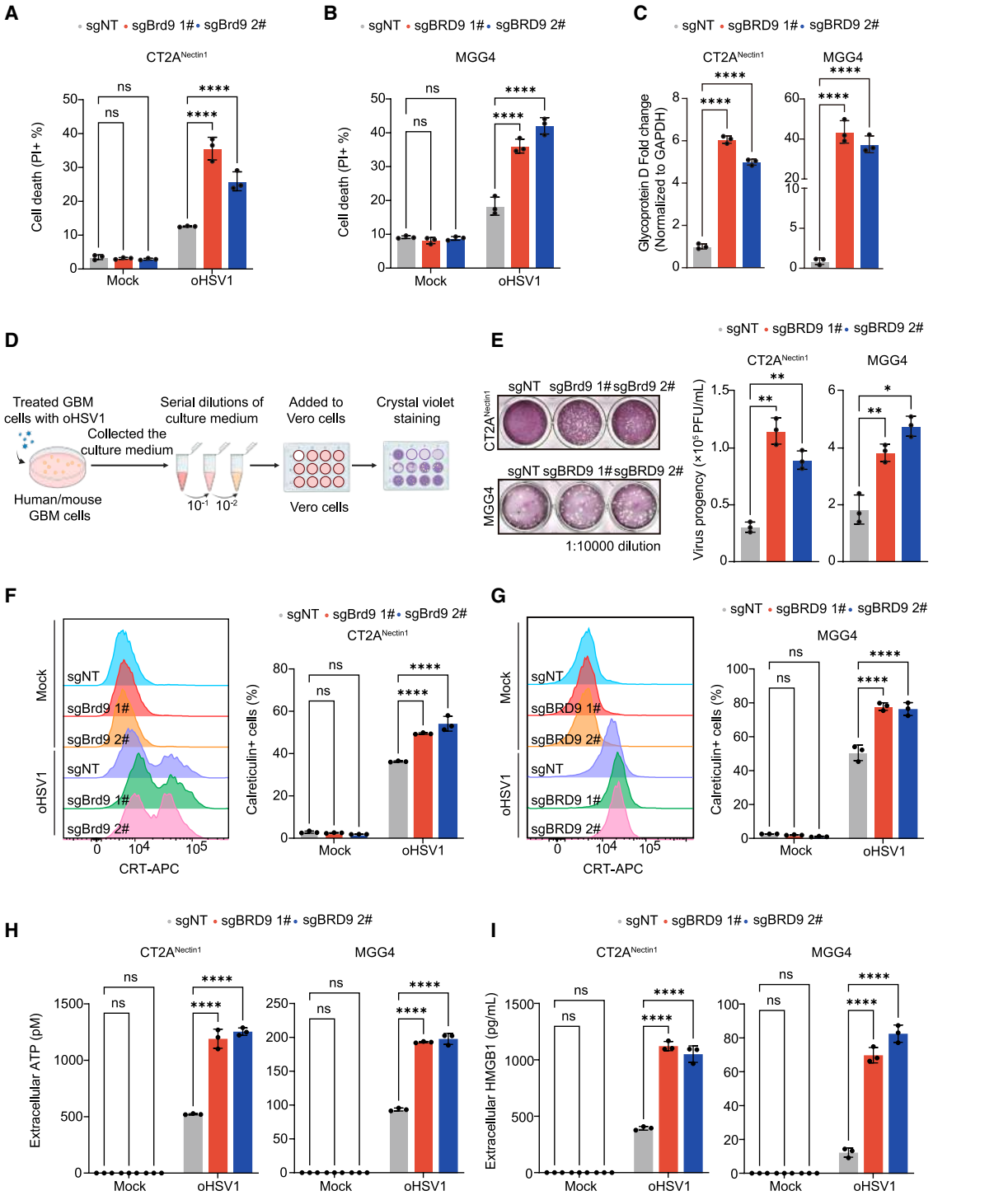

Figure 2. Knockout of BRD9 enhances the sensitivity of glioblastoma cells to oHSV1-mediated ICD and potentiates viral replication

(A) Flow cytometry analysis of oHSV1-treated control or Brd9-deficient CT2A^{Nectin1} cells subjected to PI/Annexin V staining for cell death analysis (PI+) (n = 3).

(B) Flow cytometry analysis of oHSV1-treated control or BRD9-deficient MGG4 cells subjected to PI/Annexin V staining for cell death analysis (PI+) (n = 3).

(C) Quantitative real-time PCR analysis of oHSV1 glycoprotein D levels in oHSV1-treated control or BRD9-deficient glioma cells (CT2A^{Nectin1} and MGG4). GAPDH transcript normalization (n = 3).

(D) Schematic illustration of the plaque formation assay in Vero cells.

(E) Plaque formation assay using culture medium from oHSV1-treated control or BRD9-deficient glioma cells (CT2A^{Nectin1} and MGG4). Left: representative images of crystal violet-stained Vero cell plaques treated with different culture medium (n = 3).

(legend continued on next page)

Please cite this article in press as: Guo et al., BRD9 inhibition overcomes oncolytic virus therapy resistance in glioblastoma, Cell Reports Medicine (2025), https://doi.org/10.1016/j.xcrm.2025.102258

cell lines (Figures S3A and S3B), consistent with our CRISPR screen results. Flow cytometry analysis of Annexin V/propidium iodide (PI) staining revealed that BRD9 knockout cells exhibited increased sensitivity to oHSV1-induced cell death (Figures 2A and 2B). Quantitative PCR analysis of HSV1 glycoprotein D indicated that BRD9 knockout enhanced viral replication in glioblastoma cells (Figure 2C). Additionally, viral plaque assays showed a 2- to 3-fold increase in viral load in the culture medium from BRD9 knockout cells compared to controls (Figures 2D and 2E). Previous studies have shown that oHSV1 induces ICD in tumor cells, releasing damage-associated molecular patterns such as surface-exposed calreticulin (CRT), secreted ATP, and high-mobility group protein B1 (HMGB1), which activate dendritic cells (DCs) and T cells to stimulate an antitumor immune response.[23,24] We assessed these ICD markers and found that BRD9 knockout elevated CRT exposure, increased extracellular ATP levels, and enhanced HMGB1 release in response to oHSV1 (Figures 2F–2I). This suggests that BRD9 knockout amplifies oHSV1-induced ICD in glioblastoma cells. Furthermore, we found that BRD9 knockout enhanced the antigen cross-presentation of CT2A^{Nectin1}-OVA-B2m$^{-/-}$ tumor cells by DCs, as evidenced by increased OT-1 proliferation and activation (Figures S3C and S3D). Further examination showed that BRD9 ablation did not affect viral binding or entry abilities for host cells (Figures S3E–S3H). In summary, our findings suggest that disrupting the ncBAF complex through BRD9 knockout promotes viral replication and enhances oHSV1-induced cell death, particularly ICD, leading to an increased antitumor immune response.

Brd9 knockout enhances the antitumor activity of oHSV1 therapy *in vivo*

We then investigated whether ablation of BRD9 enhances the therapeutic potency of oHSV1 *in vivo*. We intracranially implanted Brd9 knockout or control CT2A^{Nectin1} and GL261^{Nectin1} mouse glioma cells into immunocompetent mice (C57BL/6J) followed by oHSV1 treatment. We observed markedly enhanced survival outcomes in oHSV1-treated mice bearing Brd9 knockout tumors (Figures 3A, 3B, S4A, and S4B). However, without oHSV1 treatment, there was no significant difference in survival between control tumor cell-bearing mice and Brd9 knockout tumor cell-bearing mice (Figures 3A, 3B, S4A, and S4B). Moreover, we intracranially implanted BRD9 knockout or control human patient-derived GBM cells (MGG4) into NOD.Cg-*Prkdc*^{scid} *Il2rg*^{tm1Wjl}/SzJ (NSG) mice, followed by treatment with oHSV1. Our results demonstrated prolonged survival in oHSV1-treated mice with BRD9-knockout tumors (Figure S4C). These results align with our *in vitro* data, confirming that BRD9 ablation enhances oHSV1 therapeutic efficacy without directly affecting tumor cell proliferation. Immunohistochemical staining with an anti-HSV1 antibody and quantitative real-time PCR for HSV1 genomic DNA further confirmed that Brd9 knockout enhanced HSV1 replication *in vivo* (Figures 3C and S4D–S4F).

Oncolytic virotherapy not only exerts direct cytotoxic effects on tumor cells but also elicits antitumor immune responses within the TME.[6,25] To investigate the differences in the TME between Brd9-knockout and control tumors after oHSV1 treatment, we performed both flow cytometry and single-cell RNA sequencing (scRNA-seq). Flow cytometry data revealed that Brd9 ablation promoted the fraction of T cells and type 1 conventional DCs (cDC1s), as well as reduction of tumor-associated microglia in oHSV1-treated tumors (Figures 3D and S4G). Insights from scRNA-seq further confirmed that Brd9 knockout increased the infiltration of immune cells critical for the antitumor immune response, including T cells, cDC1s, and natural killer cells (Figures 3E and S4H).

T cells play a crucial role in the antitumor immune response within oncolytic virotherapy. We observed an increased percentage of T cells in both flow cytometry and scRNA-seq data. Further analysis of T cell subsets revealed that three CD8$^+$ T cell clusters were enriched in Brd9-knockout tumors treated with oHSV1 (Figure 3F). Among these clusters, cluster C2 exhibited high expression of stem-like T cell markers, including *Lef1* and *Tcf7*. Clusters C3 and C1 expressed cytotoxic markers such as *Gzmb* and *Prf1*, with cluster C1 also displaying cell proliferation markers (*Mki67*, *Top2a*, *Stmn1*, and *Tuba1b*) (Figure 3G). Flow cytometry analysis confirmed the upregulation of both CD8$^+$ T cell infiltration and the T cell activation marker CD69, as well as the cytotoxicity marker GZMB, on infiltrating CD8$^+$ T cells in oHSV1-treated Brd9-knockout tumors (Figure 3H). We also observed an increased frequency of central memory-like CD8$^+$ T cells (defined as CD44$^+$CD62L+ in CD8$^+$ T cells) in Brd9-knockout tumors (Figure 3I). To further investigate the role of CD8$^+$ T cells in oHSV1 therapy, we conducted a CD8$^+$ T cell depletion experiment. Depletion of CD8$^+$ T cells markedly diminished the survival outcomes associated with oHSV1, highlighting the critical role of CD8$^+$ T cells in the immune response to oHSV1 (Figures S4I and S4J).

BRD9 cooperates with RELA to regulate the expression of antiviral genes

To further explore the underlying molecular mechanism, we performed bulk RNA sequencing (RNA-seq) to analyze the differences in the transcriptome between BRD9 knockout and control samples in MGG4 cells after oHSV1 treatment (Figure 4A). Pathway enrichment analysis identified significant suppression of the nuclear factor κB (NF-κB) pathway in BRD9-knockout samples (Figure 4B), which is a pathway essential for the antiviral response.[26] Gene set enrichment analysis also demonstrated that genes downregulated in the BRD9 knockout group were highly enriched in the NF-κB signaling pathway (Figure 4C). To further validate our findings, we examined the expression of

(F) Calreticulin (CRT) exposure analysis of oHSV1-treated control or Brd9-deficient CT2A^{Nectin1} cells (n = 3).
(G) Calreticulin (CRT) exposure analysis of oHSV1-treated control or BRD9-deficient MGG4 cells (n = 3).
(H) Extracellular ATP level analysis in control or BRD9-deficient glioma cells (CT2A^{Nectin1} and MGG4) treated with oHSV1 (n = 3).
(I) Extracellular HMGB1-level analysis in control or BRD9-deficient glioma cells (CT2A^{Nectin1} and MGG4) treated with oHSV1 (n = 3).
Data represent mean ± SD. Two-way ANOVA (A, B, F, G, H, and I), one-way ANOVA (C and E). The diagram (D) was created using BioRender. $^*p < 0.05$, $^{**}p < 0.01$, $^{***}p < 0.001$, $^{****}p < 0.0001$; ns, not significant.

Please cite this article in press as: Guo et al., BRD9 inhibition overcomes oncolytic virus therapy resistance in glioblastoma, Cell Reports Medicine (2025), https://doi.org/10.1016/j.xcrm.2025.102258

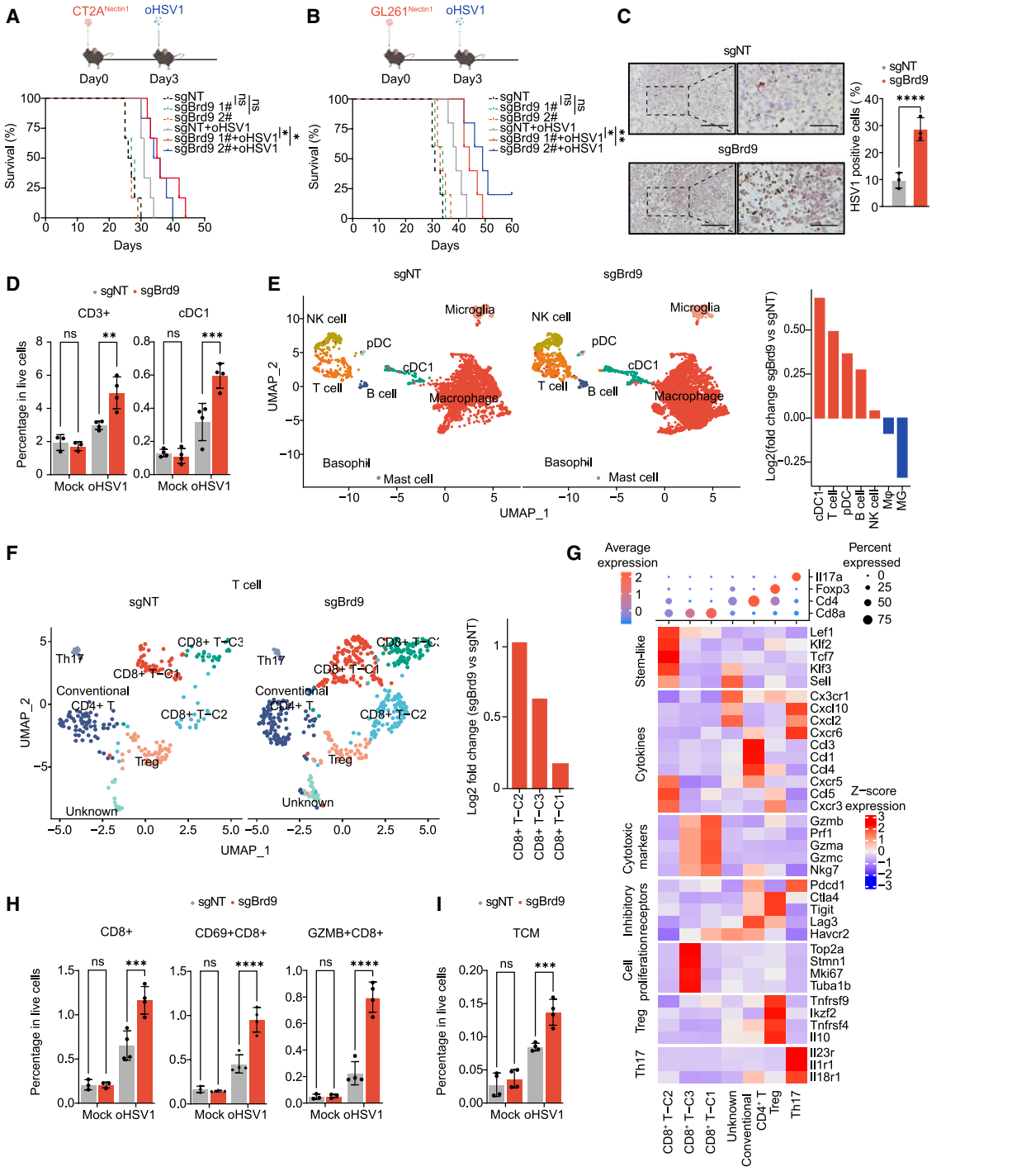

Figure 3. Knockout of Brd9 increases the efficacy of oHSV1 therapy in mouse glioma models and augments the corresponding immune cell response

(A and B) GBM mouse models were established by intracranial injection of 2×10^4 control or Brd9-deficient mouse glioma cells (CT2A^{Nectin1} and GL261^{Nectin1}) into C57BL/6J mice. 3 days later, the mice were intratumorally injected with 6×10^5 PFU of oHSV1 or mock treatment. (A) Survival curve of control or Brd9-deficient CT2A^{Nectin1} tumor-bearing mice treated with oHSV1 or mock treatment ($n = 6$). (B) Survival curve of control or Brd9-deficient GL261^{Nectin1} tumor-bearing mice treated with oHSV1 or mock treatment ($n = 6$).

(C) Analysis of oHSV1 replication in the brains of control or Brd9-deficient CT2A^{Nectin1} tumor-bearing mice. The samples were collected 2 days after intratumoral injection with 6×10^5 PFU of oHSV1; the distribution of oHSV1 in the tumors was detected via anti-HSV1 immunohistochemistry. Scale bars, left, 100 μm; right, 50 μm; ($n = 3$).

(legend continued on next page)

Please cite this article in press as: Guo et al., BRD9 inhibition overcomes oncolytic virus therapy resistance in glioblastoma, Cell Reports Medicine (2025), https://doi.org/10.1016/j.xcrm.2025.102258

several NF-κB signaling downstream antiviral response genes, including *BST2*, *ISG20*, and *OPTN*,[27–29] via quantitative real-time PCR. Consistent with the RNA-seq results, BRD9 knockout prevented the increase in the expression of these genes following oHSV1 infection (Figures 4D and S5A). To investigate whether BRD9 directly regulates the expression of these genes, we performed BRD9 chromatin immunoprecipitation sequencing (ChIP-seq). Approximately 60% of the genes downregulated by BRD9 knockout, according to the RNA-seq data, were found to be directly bound by BRD9 (Figure 4E). These BRD9-bound genes were also enriched in the NF-κB signaling pathway (Figure 4F). Driven by the consistent pathway enrichment observed in both RNA-seq and ChIP-seq data, we hypothesized that BRD9 might modulate antiviral-related genes via interaction with RELA, the key transcription factor in the NF-κB signaling pathway. Our ChIP-seq data confirmed the binding of BRD9 with RELA (Figure 4G), particularly for specific antiviral genes (Figures 4H and S5B). Subsequently, coimmunoprecipitation (coIP) was employed to further substantiate the physical interaction between BRD9 and RELA (Figure 4I). Interestingly, our CRISPR screen data further revealed that RELA knockout increased tumor cell sensitivity to oHSV1 infection, a phenotype consistent with that of BRD9 knockout (Figure 4J). Further validation confirmed that either RELA knockout or treatment with the RELA inhibitor SC75741 enhanced oHSV1-mediated cell death and increased viral replication (Figures 4K–4M, S5C, and S5D). RELA knockout or inhibition also reduced the expression of the same antiviral response genes, including *BST2*, *ISG20*, and *OPTN*, as those regulated by BRD9 (Figures 5N and S5E). In summary, our results suggest that BRD9 interacts with RELA and upregulates the expression of downstream antiviral genes.

Pharmaceutically targeting BRD9 enhances the antitumor effect of oHSV1

We then investigated the potential of pharmaceutically targeting BRD9 to augment the antitumor efficacy of oHSV1. Several BRD9 inhibitors or proteolysis-targeting chimera degraders have been developed recently, including IBRD9 and CFT8634.[21,22] We then treated human and mouse glioblastoma cells with IBRD9, followed by treatment with oHSV1. We found that BRD9 inhibition increased oHSV1-induced cytotoxicity in both cell types (Figure 5A). Moreover, BRD9 inhibition enhanced virus replication and increased virus production (Figures 5B and 5C). Furthermore, IBRD9 treatment also augmented oHSV1-induced ICD in glioblastoma cells, indicated by surface-exposed CRT, extracellular ATP, and HMGB1 release (Figures 5D–5G). These findings suggest that BRD9 inhibition amplifies oHSV1-induced cell death, particularly ICD, and promotes viral replication in tumor cells. We next performed the cross-presentation experiment to further determine whether IBRD9 could improve the antitumor immune response in combination with oHSV1 treatment. Our findings indicate that inhibition of BRD9 enhances antigen cross-presentation by DCs of CT2A^{Nectin1}-OVA-B2m$^{-/-}$ tumor cells, as evidenced by increased OT-1 proliferation (Figure 5H).

To bridge the gap between *in vitro* cell lines and the complexities of primary tumor tissues, we employed glioblastoma patient-derived organoids and primary tumor slices to investigate the impact of BRD9 inhibition on oHSV1-mediated cytotoxicity and virus replication in these *ex vivo* models.[30,31] Surgical samples obtained from patients with glioblastoma were used to generate organoids, which were subsequently treated with IBRD9 and oHSV1 (Figure 5I). PI staining and luminescent-based organoid viability assays revealed enhanced cytotoxicity upon combination treatment with IBRD9 and oHSV1 in GBM organoids (Figures 5J and 5K). Moreover, the release of ATP and HMGB1 demonstrated that treatment with IBRD9 and HSV1 enhanced the HSV1-induced ICD in human glioblastoma organoids (Figures 5L and 5M). Then, we utilized patient-derived human glioblastoma slices to evaluate the function of IBRD9 in viral infection (Figure 5N). Treatment with IBRD9 and oHSV1 enhanced virus replication in human glioblastoma slices, as evidenced by anti-HSV1 staining and HSV1 glycoprotein D qPCR results (Figures 5O–5Q).

In our *in vivo* tumor assessments, IBRD9 treatment alone did not exert a notable impact on mouse survival. Intriguingly, combination therapy using oHSV1 and IBRD9 significantly enhanced mouse survival outcomes (Figures 6A and 6B). Additionally, analysis of T cell proportions and functional markers (CD69 and GZMB) in combination treatment with IBRD9 and oHSV1 revealed higher fraction of CD8$^+$ T cells and functional marker

(D) Flow cytometry analysis of the percentages of CD3$^+$ T cells and cDC1s (CD11c+MHCII+XCR1+) in the control or Brd9-deficient CT2A^{Nectin1} tumor samples within oHSV1 treatment (n = 3 in mock group and n = 4 in oHSV1 treatment group).
(E) scRNA-seq analysis of CD45$^+$ cells from oHSV1-treated control or Brd9-deficient CT2A^{Nectin1} tumor-bearing mice. The CD45$^+$ tumor-infiltrating leukocytes were sorted with anti-mouse CD45 magnetic beads and combined in equal numbers within the same groups for 10× Genomics scRNA-seq (n = 4 mice per group). Uniform manifold approximation and projection (UMAP) plot of the scRNA-seq data depicting the different immune cell subsets (left). The proportion of cells in each cluster in the oHSV1-treated Brd9 deficiency group vs. the oHSV1-treated control group (right). Positive values indicate an increase in cluster occupancy following Brd9 deficiency.
(F) UMAP plot of T cell subclusters (left). The proportion of cells in each subcluster in the oHSV1-treated Brd9-deficient group vs. the oHSV1-treated control group (right). Positive values indicate an increase in cluster occupancy following Brd9 deficiency.
(G) Characterization of clusters with functional T cell markers. Dot plot shows the average expression levels and cell expression proportions of selected T cell marker genes (top); larger dots indicate a higher proportion of cells with expression, and red versus blue indicates higher expression. Heatmap shows the scaled expression of T cell functional markers (bottom).
(H) Flow cytometry analysis of the percentages of CD8$^+$ T cells and CD8$^+$ T cells expressing functional markers (CD69 and GZMB) in the control or Brd9-deficient CT2A^{Nectin1} tumor samples within oHSV1 treatment (n = 3 in mock group and n = 4 in oHSV1 treatment group).
(I) Flow cytometry analysis of the percentage of central memory CD8$^+$ T cells (TCM, identified as CD44$^+$ and CD62L+ in CD8$^+$ cells) in the control or Brd9-deficient CT2A^{Nectin1} tumor samples within oHSV1 treatment (n = 4).
Data represent mean ± SD. Log rank test (A and B), unpaired two-tailed Student's t test (C), two-way ANOVA (D, H, and I). *p < 0.05, **p < 0.01, ***p < 0.001, ****p < 0.0001; ns, not significant.

Please cite this article in press as: Guo et al., BRD9 inhibition overcomes oncolytic virus therapy resistance in glioblastoma, Cell Reports Medicine (2025), https://doi.org/10.1016/j.xcrm.2025.102258

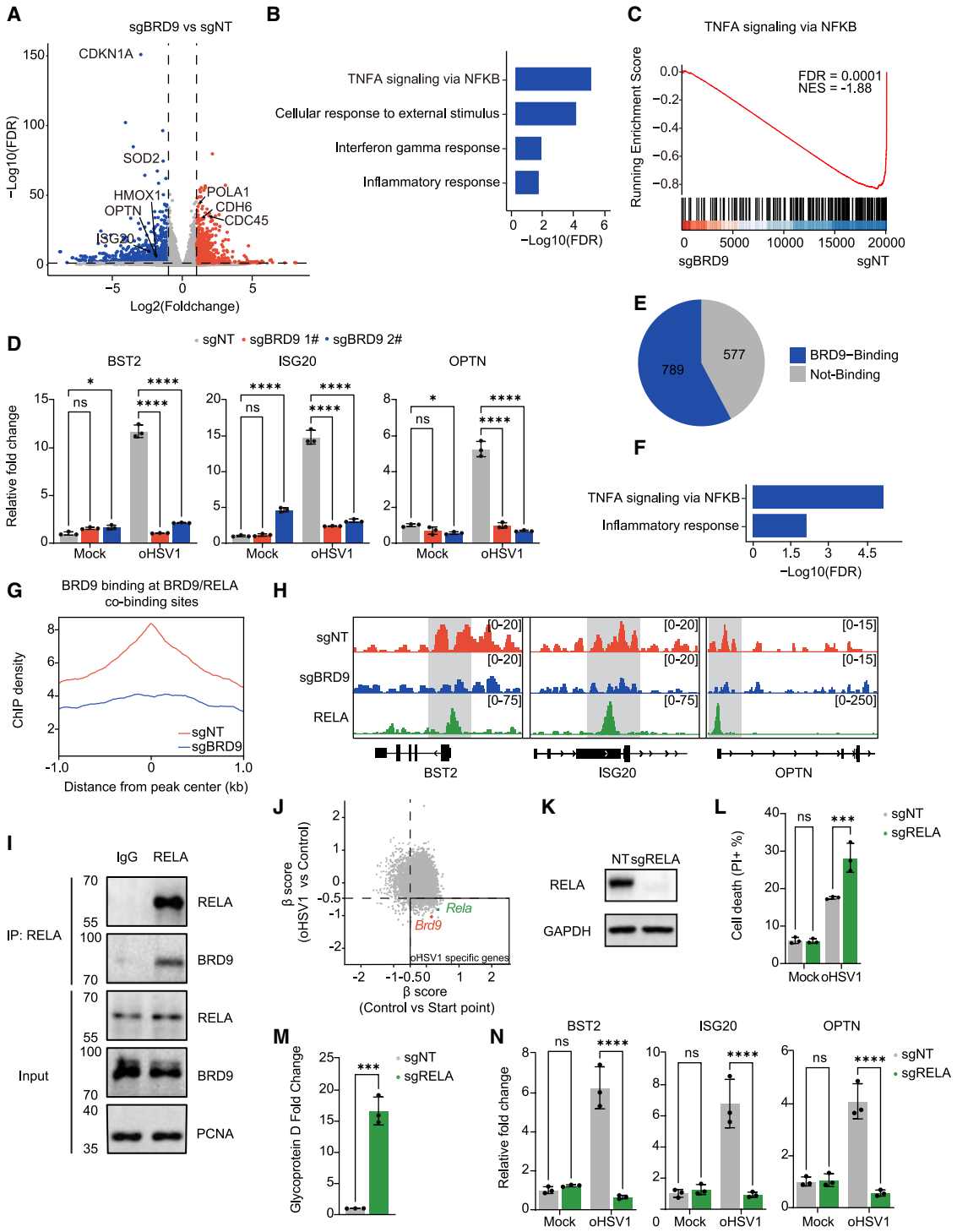

Figure 4. BRD9 interacts with RELA to regulate antiviral gene expression

(A) Volcano plot illustrating differential gene expression between oHSV1-treated control MGG4 cells and oHSV1-treated BRD9 knockout MGG4 cells. Genes with log2(fold change) > 1 and false discovery rate (FDR) < 0.05 are marked in red. Genes with log2(fold change) < −1 and FDR < 0.05 are marked in blue. Other genes are marked in gray.

(B) Pathway enrichment analysis of genes downregulated in BRD9 knockout MGG4 cells following oHSV1 treatment.

(C) Gene set enrichment analysis (GSEA) of TNFA signaling via NFKB pathway in oHSV1-treated BRD9 knockout MGG4 group vs. oHSV1-treated control MGG4 group.

(legend continued on next page)

Please cite this article in press as: Guo et al., BRD9 inhibition overcomes oncolytic virus therapy resistance in glioblastoma, Cell Reports Medicine (2025), https://doi.org/10.1016/j.xcrm.2025.102258

expression in tumors from IBRD9 and oHSV1 dual-treated mice than in those from mice treated solely with oHSV1 (Figure S6A). The efficacy of combining immune checkpoint blockade (ICB) with the oncolytic virus has been well documented, leading to corresponding clinical trials.[25,32] In our experiments, triple combination therapy involving IBRD9, oHSV1, and ICB using anti-mouse programmed cell death protein 1 (PD-1) and anti-mouse cytotoxic T-lymphocyte-associated protein 4 (CTLA-4) exhibited markedly superior antitumor effects compared to any mono- or dual-combination therapy (Figures 6A and 6B). Remarkably, this triple therapy regimen almost entirely eradicated the tumors (Figures 6A and 6B). To model the inevitable tumor recurrence observed in patients with GBM and assess the antitumor efficacy of central memory-like T cells, we rechallenged long-term survivor mice that had received triple combination therapy 60 days after the initial tumor implantation. Age-matched control mice succumbed to the two mouse tumor models within 1 month, whereas long-term survivors exhibited significant protection against tumor rechallenge, with 4 of 5 mice achieving tumor regression in the CT2A^{Nectin1} mouse model (Figure 6C) or complete tumor regression in the GL261^{Nectin1} mouse model (Figure 6D).

To further elucidate the clinical implications of our findings, we analyzed RNA-seq data and progression-free survival (PFS) data obtained from patients with glioblastoma enrolled in a recently published oHSV1 clinical trial for patients with GBM[9] (NCT03152318). Notably, lower expression levels of *BRD9* mRNA significantly correlated with prolonged PFS (Figure 6E). Beyond glioblastoma, immunohistochemistry analysis of BRD9 protein levels in liver and pancreatic cancer samples from an oHSV1 clinical trial further demonstrated that reduced BRD9 expression was associated with improved clinical outcomes[33] (NCT04806464) (Figures 6F and 6G). These findings suggest that BRD9 may serve not only as a therapeutic target for combination therapy with oncolytic viruses, but also as a prognostic biomarker for predicting treatment outcomes in oncolytic virotherapy.

DISCUSSION

Despite the considerable advances and promising outcomes in oncolytic virus therapy for cancer treatment, its overall response rate and antitumor efficacy have been limited.[10] One of the major hurdles lies in tumor-intrinsic factors that determine resistance to oncolytic viruses.[34,35] By leveraging a comprehensive whole-genome CRISPR-Cas9 knockout screen, we discovered that the ncBAF complex is a pivotal regulator of such resistance. Genetic or pharmacological disruption of BRD9, a unique subunit of the ncBAF complex, markedly augments the replication and antitumor potency of oncolytic viruses. These findings are further supported by clinical data demonstrating an inverse correlation between BRD9 expression and oncolytic virus treatment success. Consequently, our findings identify BRD9 as a potential predictive biomarker for the clinical outcomes of oncolytic virotherapy and demonstrate that combination therapies incorporating oncolytic viruses and BRD9 inhibitors hold significant promise for advancing the development of effective therapeutic strategies in glioblastoma.

Several existing studies have aimed to enhance oncolytic virus infection and replication within tumor cells by modifying the virus structure, thereby improving antitumor efficacy.[36–39] In contrast, we achieved significant enhancement of oncolytic virus replication within tumor cells by simply treating them with BRD9 inhibitors. This approach mitigates the potential toxic side effects associated with prolonged virus activation. The immunosuppressive TME of GBM tumors also plays a pivotal role in limiting the antitumor effect of oncolytic viruses.[40] Notably, previous studies have shown that BRD9 supports regulatory T (Treg) cell function by upregulating Foxp3 expression.[41] These findings indicate that combining a BRD9 inhibitor with oncolytic virus therapy may provide a dual advantage: enhancing CD8$^+$ T cell activation while attenuating Treg cell function, thereby reshaping the immunosuppressive TME to support a more robust antitumor immune response.

Our research mainly employed GBM as our experimental model for evaluating oncolytic virus therapy; the translational implications of our findings extend beyond brain tumors. Interestingly, we found that clinical trial data on oncolytic virus therapy for liver and pancreatic cancers also reveal a consistent inverse correlation between BRD9 expression and therapeutic response rates. This observation underscores the potential of BRD9 as a target for combination therapies across a variety of tumor types. In our study, we harnessed oncolytic viruses derived from HSV1. In addition to HSV1, other oncolytic viruses, such as adenovirus

(D) Quantitative real-time PCR analysis of antiviral gene (*BST2*, *ISG20*, and *OPTN*) expression in control and BRD9-deficient MGG4 cells upon oHSV1 treatment. GAPDH transcript normalization ($n = 3$).
(E) Pie chart representing BRD9 binding to genes that were significantly downregulated in BRD9 knockout cells after oHSV1 infection, as determined by BRD9 ChIP-seq.
(F) Pathway enrichment analysis of BRD9 binding to genes that were significantly downregulated in BRD9 knockout cells after oHSV1 treatment.
(G) Histogram representation of ChIP read density (±1 kb) at BRD9 and RELA common binding sites in control and BRD9 knockout MGG4 cells.
(H) Genome browser tracks of BRD9 ChIP-seq signals and RELA ChIP-seq signals (GSM2394420) at *BST2*, *ISG20*, and *OPTN* loci.
(I) CoIP analysis of the interaction between RELA and BRD9 in nuclear extracts from MGG4 cells.
(J) Scatterplot for the β scores of each gene in the oHSV1 treatment vs. the control comparison and the control vs. start point comparison. *Rela* (green) and *Brd9* (red) are highlighted.
(K) Western blot analysis of the RELA knockout efficiency in MGG4 cells.
(L) Flow cytometry analysis of cell death in oHSV1-treated control or RELA-deficient MGG4 cells, as indicated by PI/Annexin V staining (PI+) ($n = 3$).
(M) Quantitative real-time PCR analysis of oHSV1 glycoprotein D levels in control or RELA-deficient MGG4 cells following oHSV1 treatment. GAPDH transcript normalization ($n = 3$).
(N) Quantitative real-time PCR analysis of antiviral genes (*BST2*, *ISG20*, and *OPTN*) in control or RELA-deficient MGG4 cells following oHSV1 treatment. GAPDH transcript normalization ($n = 3$).
Data represent mean ± SD. Two-way ANOVA (D, L, and N) and unpaired Student's t test (M). $^*p < 0.05$, $^{**}p < 0.01$, $^{***}p < 0.001$, $^{****}p < 0.0001$; ns, not significant.

Please cite this article in press as: Guo et al., BRD9 inhibition overcomes oncolytic virus therapy resistance in glioblastoma, Cell Reports Medicine (2025), https://doi.org/10.1016/j.xcrm.2025.102258

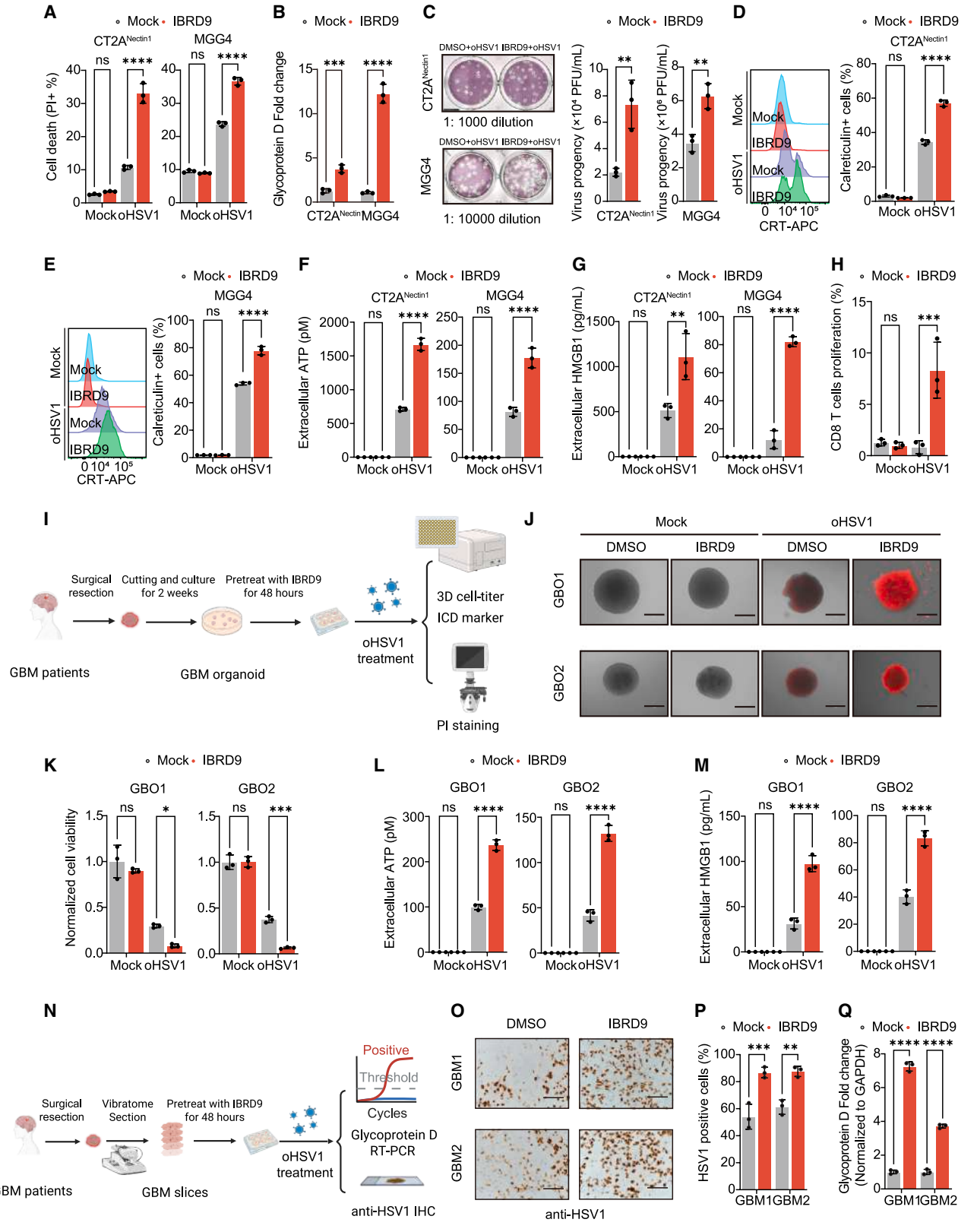

(legend on next page)

Please cite this article in press as: Guo et al., BRD9 inhibition overcomes oncolytic virus therapy resistance in glioblastoma, Cell Reports Medicine (2025), https://doi.org/10.1016/j.xcrm.2025.102258

and poliovirus, are currently being investigated in clinical trials for glioblastoma treatment and have demonstrated promising outcomes.[42,43] It has been reported that BRD9 can enhance the interferon (IFN) response genes expression, subsequently inhibiting the replication of various viruses.[44] Taking together, our study identified a different molecular mechanism by which BRD9 modulates oncolytic virus resistance, specifically through the NF-κB pathway, rather than the previously reported IFN signaling, which is often inactive or downregulated in many types of cancers including glioblastoma.[45–47] Hence, targeting BRD9 could potentially enhance the therapeutic effects of various oncolytic viruses in a wide range of cancer types, a prospect that warrants further exploration in future studies.

Limitations of the study

In the current study, we focused solely on glioblastoma tumor models to assess the therapeutic efficacy of oncolytic viruses. Future studies should include a broader array of tumor models to determine whether the enhancement of oncolytic viruses via BRD9 inhibition holds true across different tumor types. Moreover, our study primarily employed an immunocompetent mouse model, which may not fully replicate the complexities of human cancer. Incorporating humanized mouse models with patient-derived xenografts in future research would improve the translational relevance and applicability of these findings. Future studies will strengthen the translational relevance of this finding.

RESOURCE AVAILABILITY

Lead contact

Further information and request for resources and reagents should be directed to and will be fulfilled by the lead contact, Qi Xie (xieqi@westlake.edu.cn).

Materials availability

This study did not generate new unique reagents.

Data and code availability

- Bulk RNA-seq and scRNA-seq data reported in this paper have been deposited into the National Center for Biotechnology Information Sequence Read Archive under accession number PRJNA1066491. BRD9 ChIP-seq data can be downloaded from the Gene Expression Omnibus website, accession number GEO: GSE260886. Gene expression and survival data of the phase 1 trial of patients with glioblastoma treated with CAN-3110 (aka rQNestin34.5v.2) were downloaded from the dbGap (phs003378.v1.p1). ChIP-seq data for RELA used in this study were retrieved from GSM2394420.
- The custom code used for this paper is available on GitHub at the following address: https://github.com/Dragonlongzhilin/OV_BRD9.
- Any additional information required to reanalyze the data reported in this work paper is available from the lead contact upon request.

ACKNOWLEDGMENTS

We thank Dr. Hiroaki Wakimoto (Massachusetts General Hospital) for kindly providing the MGG4 GSC line. We thank Dr. Jeremy Rich (University of Pittsburgh) for kindly providing the GSC3264 GSC line and neural progenitor cell lines (ENSA and hNP1). We thank Dr. Kai Lei (Westlake University) for kindly providing the human ES cell line H1. We thank all technicians at the Westlake University facilities for their technical assistance. We also thank Westlake University Language Center for manuscript editing. The GBM oHSV1 clinical trial data used in this study were obtained from dbGaP with accession number phs003378. We acknowledge the Submitting Investigator(s) who contributed the data, the primary funding organization that supported the Submitting Investigator(s), and the NIH-designated data repository. This work was supported by grants from the National Natural Science Foundation of China (nos. 31971364 and 32370148), the National Key R&D Program of China (2022YFC3400205), and the Science and Technology Innovation Action Plan of Shanghai (24Z510200306) to Y.C. This work was supported by CAMS Innovation Fund for Medical Science (CIFMS, 2023-I2M-2-010) to C. Wang. This work was supported by grants from the National Natural Science

Figure 5. Pharmaceutically targeting BRD9 enhances the antitumor effect of oHSV1 *in vitro*

(A) Flow cytometry analysis of oHSV1-treated control or IBRD9-pretreated (1 μM, 24 h) CT2A^{Nectin1} and MGG4 cells subjected to PI/Annexin V staining for cell death analysis (PI+) (n = 3).

(B) Quantitative real-time PCR analysis of oHSV1 glycoprotein D levels in control or IBRD9-pretreated (1 μM, 24 h) CT2A^{Nectin1} and MGG4 cells treated with oHSV1. GAPDH/Gapdh transcript normalization (n = 3).

(C) Plaque formation assay of oHSV1-treated control or IBRD9-pretreated (1 μM, 24 h) CT2A^{Nectin1} and MGG4 cell culture medium. The virus titer was determined after 48 h (n = 3).

(D) Calreticulin (CRT) exposure analysis of control or IBRD9-pretreated (1 μM, 24 h) CT2A^{Nectin1} cells treated with oHSV1 (n = 3).

(E) Calreticulin (CRT) exposure analysis of control or IBRD9-pretreated (1 μM, 24 h) MGG4 cells treated with oHSV1 (n = 3).

(F) Extracellular ATP level analysis in control or IBRD9-pretreated (1 μM, 24 h) CT2A^{Nectin1} and MGG4 cells treated with oHSV1 (n = 3).

(G) Extracellular HMGB1 level analysis in control or IBRD9-pretreated (1 μM, 24 h) CT2A^{Nectin1} and MGG4 cells treated with oHSV1 (n = 3).

(H) *In vitro* co-culture proliferation experiments with OT-I CD8$^+$ T cells and cDC1s generated from WT mice in the IBRD9- and oHSV1-treated CT2A^{Nectin1}-OVA-B2m$^{-/-}$ cells (n = 3).

(I) Schematic of human glioblastoma-derived organoid processing and verification of oHSV1-mediated killing by PI staining, 3D cell titer assays, and ICD marker analysis.

(J) PI staining of IBRD9-pretreated (1 μM, 24 h) human glioblastoma-derived organoids treated with oHSV1. Scale bars, 300 μm.

(K) 3D cell viability assay of IBRD9-pretreated (1 μM, 24 h) human glioblastoma-derived organoids treated with oHSV1 (n = 3).

(L) Extracellular ATP-level analysis in control or IBRD9-pretreated (1 μM, 24 h) human glioblastoma-derived organoids treated with oHSV1 (n = 3).

(M) Extracellular HMGB1-level analysis in control or IBRD9-pretreated (1 μM, 24 h) human glioblastoma-derived organoids treated with oHSV1 (n = 3).

(N) Schematic of human glioblastoma-derived tumor slice processing and verification of oHSV1 replication by anti-HSV1 staining and quantitative real-time PCR.

(O) Representative immunohistochemistry images of HSV1 staining in IBRD9-pretreated or control human glioblastoma-derived tumor slices. Scale bars, 50 μm.

(P) Analysis of oHSV1 replication in IBRD9-pretreated (2 μM, 24 h) or control human glioblastoma-derived tumor slices. After oHSV1 treatment, the distribution of oHSV1 in the sections was detected by anti-HSV1 immunohistochemistry (n = 3).

(Q) Quantitative real-time PCR analysis of oHSV1 glycoprotein D levels in control or IBRD9-pretreated (2 μM, 24 h) human glioblastoma-derived tumor sections treated with oHSV1. GAPDH transcript normalization (n = 3).

Data represent mean ± SD. Two-way ANOVA (A, D, E, F, G, H, K, L, and M), unpaired two-tailed Student's t test (B, C, P, and Q). The diagrams (I and N) were created using BioRender. *p < 0.05, **p < 0.01, ***p < 0.001, ****p < 0.0001; ns, not significant.

Please cite this article in press as: Guo et al., BRD9 inhibition overcomes oncolytic virus therapy resistance in glioblastoma, Cell Reports Medicine (2025), https://doi.org/10.1016/j.xcrm.2025.102258

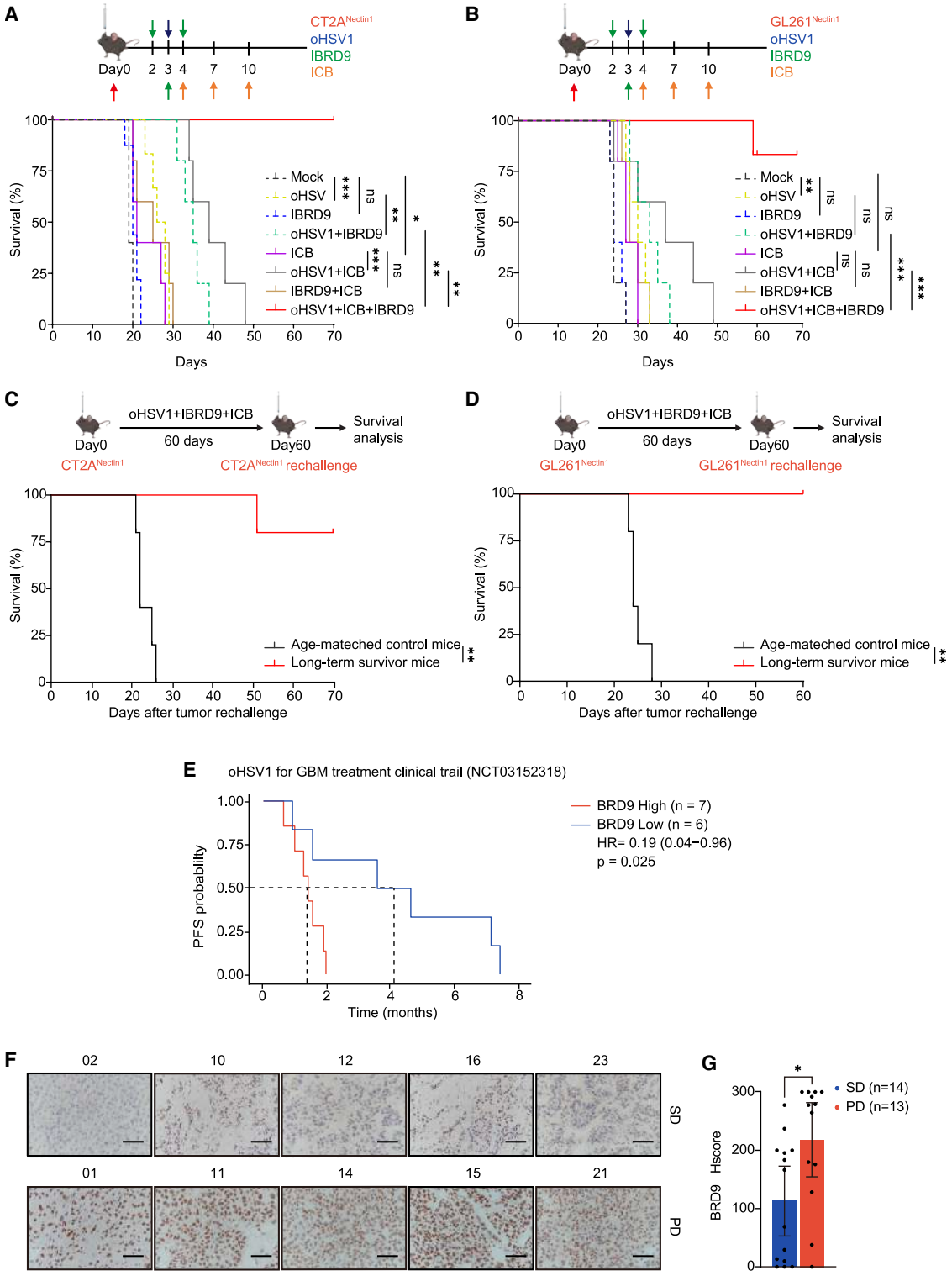

Figure 6. Pharmaceutically targeting BRD9 enhances the antitumor effect of oHSV1 *in vivo*, and BRD9 expression is associated with poor clinical outcome in cancer patients treated with oHSV1

(A) Survival curve of IBRD9, oHSV1, and ICB (the anti-mouse PD-1 antibody and the anti-mouse CTLA4 antibody) combination therapy in CT2A^{Nectin1} tumor-bearing mice (n = 5).

(B) Survival curve of IBRD9, oHSV1, and ICB (the anti-mouse PD-1 antibody and the anti-mouse CTLA4 antibody) combination therapy in GL261^{Nectin1} tumor-bearing mice (n = 5).

(legend continued on next page)

Foundation of China (82473121 and 82073268) and Westlake Education Foundation to Q.X. We also thank the "Pioneer" and "Leading Goose" R&D Program of Zhejiang (2024SSYS0036) for supporting this work.

AUTHOR CONTRIBUTIONS

Q.X. and C. Wang. conceived the project and supervised the experimental design. C.G., J. Yu., J. Yang., P.L., S.Z., Z.X., C. Wu., and W.Z. performed or assisted with the experiments. C.G., Z.L., and X.R. analyzed the data. Y. S., Y.M., F.L., and J.Z. provided the critical reagents. Y.C. and Y.Z. provided the oHSV1. Q.X., C. Wang., C.G., and Z.L. interpreted the results and co-wrote the manuscript. All authors critically read and approved the final paper.

DECLARATION OF INTERESTS

Y.C. is a co-founder and advisor of BDgene Therapeutics.

STAR★METHODS

Detailed methods are provided in the online version of this paper and include the following:

SUPPLEMENTAL INFORMATION

Supplemental information can be found online at https://doi.org/10.1016/j.xcrm.2025.102258.

Received: March 27, 2025
Revised: June 4, 2025
Accepted: July 3, 2025

REFERENCES

1. Ostrom, Q.T., Price, M., Neff, C., Cioffi, G., Waite, K.A., Kruchko, C., and Barnholtz-Sloan, J.S. (2023). CBTRUS Statistical Report: Primary Brain and Other Central Nervous System Tumors Diagnosed in the United States in 2016—2020. Neuro Oncol. *25*, iv1–iv99. https://doi.org/10.1093/neuonc/noad149.
2. Wu, W., Klockow, J.L., Zhang, M., Lafortune, F., Chang, E., Jin, L., Wu, Y., and Daldrup-Link, H.E. (2021). Glioblastoma multiforme (GBM): An overview of current therapies and mechanisms of resistance. Pharmacol. Res. *171*, 105780. https://doi.org/10.1016/j.phrs.2021.105780.
3. Nduom, E.K., Weller, M., and Heimberger, A.B. (2015). Immunosuppressive mechanisms in glioblastoma: Fig. 1. Neuro Oncol. *17*, vii9–vii14. https://doi.org/10.1093/neuonc/nov151.
4. Lim, M., Xia, Y., Bettegowda, C., and Weller, M. (2018). Current state of immunotherapy for glioblastoma. Nat. Rev. Clin. Oncol. *15*, 422–442. https://doi.org/10.1038/s41571-018-0003-5.
5. Jackson, C.M., Choi, J., and Lim, M. (2019). Mechanisms of immunotherapy resistance: lessons from glioblastoma. Nat. Immunol. *20*, 1100–1109. https://doi.org/10.1038/s41590-019-0433-y.
6. Kaufman, H.L., Kohlhapp, F.J., and Zloza, A. (2015). Oncolytic viruses: a new class of immunotherapy drugs. Nat. Rev. Drug Discov. *14*, 642–662. https://doi.org/10.1038/nrd4663.
7. Todo, T., Ino, Y., Ohtsu, H., Shibahara, J., and Tanaka, M. (2022). A phase I/II study of triple-mutated oncolytic herpes virus G47Δ in patients with progressive glioblastoma. Nat. Commun. *13*, 4119. https://doi.org/10.1038/s41467-022-31262-y.
8. Todo, T., Ito, H., Ino, Y., Ohtsu, H., Ota, Y., Shibahara, J., and Tanaka, M. (2022). Intratumoral oncolytic herpes virus G47Δ for residual or recurrent glioblastoma: a phase 2 trial. Nat. Med. *28*, 1630–1639. https://doi.org/10.1038/s41591-022-01897-x.
9. Ling, A.L., Solomon, I.H., Landivar, A.M., Nakashima, H., Woods, J.K., Santos, A., Masud, N., Fell, G., Mo, X., Yilmaz, A.S., et al. (2023). Clinical trial links oncolytic immunoactivation to survival in glioblastoma. Nature *623*, 157–166. https://doi.org/10.1038/s41586-023-06623-2.
10. Shalhout, S.Z., Miller, D.M., Emerick, K.S., and Kaufman, H.L. (2023). Therapy with oncolytic viruses: progress and challenges. Nat. Rev. Clin. Oncol. *20*, 160–177. https://doi.org/10.1038/s41571-022-00719-w.

(C) Survival curve of long-term survivor mice and age-matched control mice challenged with $CT2A^{Nectin1}$ cells ($n = 5$).
(D) Survival curve of long-term survivor mice and age-matched control mice challenged with $GL261^{Nectin1}$ cells ($n = 5$).
(E) Kaplan-Meier analysis showing the PFS of patients with glioblastoma treated with oHSV1 subdivided by the expression of BRD9 (high-expression patients: $n = 7$; low-expression patients: $n = 6$). HR, hazard ratio.
(F) Analysis of BRD9 expression in liver cancer and pancreatic cancer biopsy sections from patients participating in an oHSV1 clinical trial. Representative immunohistochemistry images of BRD9 staining (oHSV1 response: SD, stable disease; oHSV1 nonresponse: PD, progressive disease). Scale bars, 50 μm.
(G) BRD9-stained sections were quantified by H-score (SD: $n = 14$; PD: $n = 13$).
Data represent mean ± SD. Unpaired two-tailed Student's t test (G) and log rank test (A–E). $^{*}p < 0.05$, $^{**}p < 0.01$, $^{***}p < 0.001$, $^{****}p < 0.0001$; ns, not significant.

11. Nguyen, H.-M., and Saha, D. (2021). The Current State of Oncolytic Herpes Simplex Virus for Glioblastoma Treatment. Oncolytic Virother. *10*, 1–27. https://doi.org/10.2147/ov.S268426.

12. Mohr, I., Sternberg, D., Ward, S., Leib, D., Mulvey, M., and Gluzman, Y. (2001). A Herpes Simplex Virus Type 1 γ34.5 Second-Site Suppressor Mutant That Exhibits Enhanced Growth in Cultured Glioblastoma Cells Is Severely Attenuated in Animals. J. Virol. *75*, 5189–5196. https://doi.org/10.1128/jvi.75.11.5189-5196.2001.

13. Liu, B.L., Robinson, M., Han, Z.Q., Branston, R.H., English, C., Reay, P., McGrath, Y., Thomas, S.K., Thornton, M., Bullock, P., et al. (2003). ICP34.5 deleted herpes simplex virus with enhanced oncolytic, immune stimulating, and anti-tumour properties. Gene Ther. *10*, 292–303. https://doi.org/10.1038/sj.gt.3301885.

14. Ripa, I., Andreu, S., López-Guerrero, J.A., and Bello-Morales, R. (2022). Interplay between Autophagy and Herpes Simplex Virus Type 1: ICP34.5, One of the Main Actors. Int. J. Mol. Sci. *23*, 13643. https://doi.org/10.3390/ijms232113643.

15. Zhong, Y., Le, H., Zhang, X., Dai, Y., Guo, F., Ran, X., Hu, G., Xie, Q., Wang, D., and Cai, Y. (2024). Identification of restrictive molecules involved in oncolytic virotherapy using genome-wide CRISPR screening. J. Hematol. Oncol. *17*, 36. https://doi.org/10.1186/s13045-024-01554-5.

16. Zhang, N., Yan, J., Lu, G., Guo, Z., Fan, Z., Wang, J., Shi, Y., Qi, J., and Gao, G.F. (2011). Binding of herpes simplex virus glycoprotein D to nectin-1 exploits host cell adhesion. Nat. Commun. *2*, 267–277. https://doi.org/10.1038/ncomms1571.

17. Wang, B., Wang, M., Zhang, W., Xiao, T., Chen, C.-H., Wu, A., Wu, F., Traugh, N., Wang, X., Li, Z., et al. (2019). Integrative analysis of pooled CRISPR genetic screens using MAGeCKFlute. Nat. Protoc. *14*, 756–780. https://doi.org/10.1038/s41596-018-0113-7.

18. Hart, T., Chandrashekhar, M., Aregger, M., Steinhart, Z., Brown, K.R., MacLeod, G., Mis, M., Zimmermann, M., Fradet-Turcotte, A., Sun, S., et al. (2015). High-Resolution CRISPR Screens Reveal Fitness Genes and Genotype-Specific Cancer Liabilities. Cell *163*, 1515–1526. https://doi.org/10.1016/j.cell.2015.11.015.

19. Kim, E., and Hart, T. (2021). Improved analysis of CRISPR fitness screens and reduced off-target effects with the BAGEL2 gene essentiality classifier. Genome Med. *13*, 2. https://doi.org/10.1186/s13073-020-00809-3.

20. Mittal, P., and Roberts, C.W.M. (2020). The SWI/SNF complex in cancer — biology, biomarkers and therapy. Nat. Rev. Clin. Oncol. *17*, 435–448. https://doi.org/10.1038/s41571-020-0357-3.

21. Theodoulou, N.H., Bamborough, P., Bannister, A.J., Becher, I., Bit, R.A., Che, K.H., Chung, C.-w., Dittmann, A., Drewes, G., Drewry, D.H., et al. (2015). Discovery of I-BRD9, a Selective Cell Active Chemical Probe for Bromodomain Containing Protein 9 Inhibition. J. Med. Chem. *59*, 1425–1439. https://doi.org/10.1021/acs.jmedchem.5b00256.

22. Poling, L.L., Cocozziello, D., He, M., Hurh, E., Lobbardi, R., Jackson, K.L., Fisher, S.L., and Pollock, R.M. (2023). CFT8634, a Clinical Stage BRD9 Bi DAC™ Degrader, Is Active in a Subset of Multiple Myeloma Cell Line Models and Synergistic When Combined with Pomalidomide. Blood *142*, 6594. https://doi.org/10.1182/blood-2023-174555.

23. Palanivelu, L., Liu, C.-H., and Lin, L.-T. (2023). Immunogenic cell death: The cornerstone of oncolytic viro-immunotherapy. Front. Immunol. *13*, 1038226. https://doi.org/10.3389/fimmu.2022.1038226.

24. Krysko, D.V., Garg, A.D., Kaczmarek, A., Krysko, O., Agostinis, P., and Vandenabeele, P. (2012). Immunogenic cell death and DAMPs in cancer therapy. Nat. Rev. Cancer *12*, 860–875. https://doi.org/10.1038/nrc3380.

25. Bommareddy, P.K., Shettigar, M., and Kaufman, H.L. (2018). Integrating oncolytic viruses in combination cancer immunotherapy. Nat. Rev. Immunol. *18*, 498–513. https://doi.org/10.1038/s41577-018-0014-6.

26. Rall, G.F., Balachandran, S., and Beg, A.A. (2011). Defining Emerging Roles for NF-κB in Antivirus Responses: Revisiting the Interferon-β Enhanceosome Paradigm. PLoS Pathog. *7*, e1002165. https://doi.org/10.1371/journal.ppat.1002165.

27. Jackson, J.D., Markert, J.M., Li, L., Carroll, S.L., and Cassady, K.A. (2016). STAT1 and NF-κB Inhibitors Diminish Basal Interferon-Stimulated Gene Expression and Improve the Productive Infection of Oncolytic HSV in MPNST Cells. Mol. Cancer Res. *14*, 482–492. https://doi.org/10.1158/1541-7786.Mcr-15-0427.

28. Vij, N., Sudhakar, C., Nagabhushana, A., Jain, N., and Swarup, G. (2009). NF-κB Mediates Tumor Necrosis Factor α-Induced Expression of Optineurin, a Negative Regulator of NF-κB. PLoS One *4*, e5114. https://doi.org/10.1371/journal.pone.0005114.

29. Deymier, S., Louvat, C., Fiorini, F., and Cimarelli, A. (2022). ISG20: an enigmatic antiviral RNase targeting multiple viruses. FEBS Open Bio *12*, 1096–1111. https://doi.org/10.1002/2211-5463.13382.

30. Jacob, F., Salinas, R.D., Zhang, D.Y., Nguyen, P.T.T., Schnoll, J.G., Wong, S.Z.H., Thokala, R., Sheikh, S., Saxena, D., Prokop, S., et al. (2020). A Patient-Derived Glioblastoma Organoid Model and Biobank Recapitulates Inter- and Intra-tumoral Heterogeneity. Cell *180*, 188–204.e122. https://doi.org/10.1016/j.cell.2019.11.036.

31. Sebollela, A., Neder, L., Garcia-Cairasco, N., Assirati Junior, J.A., Horta-Junior, J.d.A.d.C., Machado, C.d.M., Nogueira, G.O., Almeida, G.M., Mendes, N.D., and Fernandes, A. (2019). Short-Term Free-Floating Slice Cultures from the Adult Human Brain. JoVE J. e59845. https://doi.org/10.3791/59845.

32. Harrington, K., Freeman, D.J., Kelly, B., Harper, J., and Soria, J.-C. (2019). Optimizing oncolytic virotherapy in cancer treatment. Nat. Rev. Drug Discov. *18*, 689–706. https://doi.org/10.1038/s41573-019-0029-0.

33. Shen, Y., Bai, X., Zhang, Q., Liang, X., Jin, X., Zhao, Z., Song, W., Tan, Q., Zhao, R., Jia, W., et al. (2025). Oncolytic virus VG161 in refractory hepatocellular carcinoma. Nature *641*, 503–511. https://doi.org/10.1038/s41586-025-08717-5.

34. Dittmer, D.P., Zakaria, C., Sean, P., Hoang, H.-D., Leroux, L.-P., Watson, M., Workenhe, S.T., Hearnden, J., Pearl, D., Truong, V.T., et al. (2018). Active-site mTOR inhibitors augment HSV1-dICP0 infection in cancer cells via dysregulated eIF4E/4E-BP axis. PLoS Pathog. *14*, e1007264. https://doi.org/10.1371/journal.ppat.1007264.

35. Nguyen, T.-T., Ramsay, L., Ahanfeshar-Adams, M., Lajoie, M., Schadendorf, D., Alain, T., and Watson, I.R. (2021). Mutations in the IFNγ-JAK-STAT Pathway Causing Resistance to Immune Checkpoint Inhibitors in Melanoma Increase Sensitivity to Oncolytic Virus Treatment. Clin. Cancer Res. *27*, 3432–3442. https://doi.org/10.1158/1078-0432.Ccr-20-3365.

36. Xu, B., Ma, R., Russell, L., Yoo, J.Y., Han, J., Cui, H., Yi, P., Zhang, J., Nakashima, H., Dai, H., et al. (2018). An oncolytic herpesvirus expressing E-cadherin improves survival in mouse models of glioblastoma. Nat. Biotechnol. *37*, 45–54. https://doi.org/10.1038/nbt.4302.

37. Xu, B., Tian, L., Chen, J., Wang, J., Ma, R., Dong, W., Li, A., Zhang, J., Antonio Chiocca, E., Kaur, B., et al. (2021). An oncolytic virus expressing a full-length antibody enhances antitumor innate immune response to glioblastoma. Nat. Commun. *12*, 5908. https://doi.org/10.1038/s41467-021-26003-6.

38. Panagioti, E., Kurokawa, C., Viker, K., Ammayappan, A., Anderson, S.K., Sotiriou, S., Chatzopoulos, K., Ayasoufi, K., Johnson, A.J., Iankov, I.D., and Galanis, E. (2021). Immunostimulatory bacterial antigen–armed oncolytic measles virotherapy significantly increases the potency of anti-PD1 checkpoint therapy. J. Clin. Investig. *131*, e141614. https://doi.org/10.1172/jci141614.

39. Tian, L., Xu, B., Chen, Y., Li, Z., Wang, J., Zhang, J., Ma, R., Cao, S., Hu, W., Chiocca, E.A., et al. (2022). Specific targeting of glioblastoma with an oncolytic virus expressing a cetuximab-CCL5 fusion protein via innate and adaptive immunity. Nat. Cancer *3*, 1318–1335. https://doi.org/10.1038/s43018-022-00448-0.

40. Rius-Rocabert, S., García-Romero, N., García, A., Ayuso-Sacido, A., and Nistal-Villan, E. (2020). Oncolytic Virotherapy in Glioma Tumors. Int. J. Mol. Sci. *21*, 7604. https://doi.org/10.3390/ijms21207604.

41. Loo, C.-S., Gatchalian, J., Liang, Y., Leblanc, M., Xie, M., Ho, J., Venkatraghavan, B., Hargreaves, D.C., and Zheng, Y. (2020). A Genome-wide

CRISPR Screen Reveals a Role for the Non-canonical Nucleosome-Remodeling BAF Complex in Foxp3 Expression and Regulatory T Cell Function. Immunity *53*, 143–157.e148. https://doi.org/10.1016/j.immuni.2020.06.011.

42. Kiyokawa, J., and Wakimoto, H. (2019). Preclinical And Clinical Development Of Oncolytic Adenovirus For The Treatment Of Malignant Glioma. Oncolytic Virother. *8*, 27–37. https://doi.org/10.2147/ov.S196403.
43. Desjardins, A., Gromeier, M., Herndon, J.E., Beaubier, N., Bolognesi, D.P., Friedman, A.H., Friedman, H.S., McSherry, F., Muscat, A.M., Nair, S., et al. (2018). Recurrent Glioblastoma Treated with Recombinant Poliovirus. N. Engl. J. Med. *379*, 150–161. https://doi.org/10.1056/NEJMoa1716435.
44. Börold, J., Eletto, D., Busnadiego, I., Mair, N.K., Moritz, E., Schiefer, S., Schmidt, N., Petric, P.P., Wong, W.W.L., Schwemmle, M., and Hale, B. G. (2021). BRD9 is a druggable component of interferon-stimulated gene expression and antiviral activity. EMBO Rep. *22*, e52823. https://doi.org/10.15252/embr.202152823.
45. Olopade, O.I., Jenkins, R.B., Ransom, D.T., Malik, K., Pomykala, H., Nobori, T., Cowan, J.M., Rowley, J.D., and Diaz, M.O. (1992). Molecular analysis of deletions of the short arm of chromosome 9 in human gliomas. Cancer Res. *52*, 2523–2529.
46. Cairns, P., Tokino, K., Eby, Y., and Sidransky, D. (1994). Homozygous deletions of 9p21 in primary human bladder tumors detected by comparative multiplex polymerase chain reaction. Cancer Res. *54*, 1422–1424.
47. Saidi, R.F., Williams, F., Silberberg, B., Mittal, V.K., ReMine, S.G., and Jacobs, M.J. (2006). Expression of interferon receptors in pancreatic cancer: identification of a novel prognostic factor. Surgery *139*, 743–748. https://doi.org/10.1016/j.surg.2005.11.010.
48. Raju, S., Botts, S.R., Blaser, M.C., Abdul-Samad, M., Prajapati, K., Khosraviani, N., Ho, T.W.W., Breda, L.C.D., Ching, C., Galant, N.J., et al. (2024). Directional Endothelial Communication by Polarized Extracellular Vesicle Release. Circ. Res. *134*, 269–289. https://doi.org/10.1161/circresaha.123.322993.
49. Kim, D., Paggi, J.M., Park, C., Bennett, C., and Salzberg, S.L. (2019). Graph-based genome alignment and genotyping with HISAT2 and HISAT-genotype. Nat. Biotechnol. *37*, 907–915. https://doi.org/10.1038/s41587-019-0201-4.
50. Liao, Y., Smyth, G.K., and Shi, W. (2014). featureCounts: an efficient general purpose program for assigning sequence reads to genomic features. Bioinformatics *30*, 923–930. https://doi.org/10.1093/bioinformatics/btt656.
51. Love, M.I., Huber, W., and Anders, S. (2014). Moderated estimation of fold change and dispersion for RNA-seq data with DESeq2. Genome Biol. *15*, 550. https://doi.org/10.1186/s13059-014-0550-8.
52. Chen, S. (2023). Ultrafast one-pass FASTQ data preprocessing, quality control, and deduplication using fastp. iMeta *2*, e107. https://doi.org/10.1002/imt2.107.
53. Langmead, B., and Salzberg, S.L. (2012). Fast gapped-read alignment with Bowtie 2. Nat. Methods *9*, 357–359. https://doi.org/10.1038/nmeth.1923.
54. Danecek, P., Bonfield, J.K., Liddle, J., Marshall, J., Ohan, V., Pollard, M.O., Whitwham, A., Keane, T., McCarthy, S.A., Davies, R.M., and Li, H. (2021). Twelve years of SAMtools and BCFtools. GigaScience *10*, giab008. https://doi.org/10.1093/gigascience/giab008.
55. Zhang, Y., Liu, T., Meyer, C.A., Eeckhoute, J., Johnson, D.S., Bernstein, B. E., Nusbaum, C., Myers, R.M., Brown, M., Li, W., and Liu, X.S. (2008). Model-based Analysis of ChIP-Seq (MACS). Genome Biol. *9*, R137. https://doi.org/10.1186/gb-2008-9-9-r137.
56. Yu, G., Wang, L.-G., and He, Q.-Y. (2015). ChIPseeker: an R/Bioconductor package for ChIP peak annotation, comparison and visualization. Bioinformatics *31*, 2382–2383. https://doi.org/10.1093/bioinformatics/btv145.
57. Ramírez, F., Ryan, D.P., Grüning, B., Bhardwaj, V., Kilpert, F., Richter, A. S., Heyne, S., Dündar, F., and Manke, T. (2016). deepTools2: a next generation web server for deep-sequencing data analysis. Nucleic Acids Res. *44*, W160–W165. https://doi.org/10.1093/nar/gkw257.
58. Thorvaldsdottir, H., Robinson, J.T., and Mesirov, J.P. (2012). Integrative Genomics Viewer (IGV): high-performance genomics data visualization and exploration. Briefings Bioinf. *14*, 178–192. https://doi.org/10.1093/bib/bbs017.
59. Fleming, S.J., Chaffin, M.D., Arduini, A., Akkad, A.-D., Banks, E., Marioni, J.C., Philippakis, A.A., Ellinor, P.T., and Babadi, M. (2023). Unsupervised removal of systematic background noise from droplet-based single-cell experiments using CellBender. Nat. Methods *20*, 1323–1335. https://doi.org/10.1038/s41592-023-01943-7.
60. Hao, Y., Hao, S., Andersen-Nissen, E., Mauck, W.M., Zheng, S., Butler, A., Lee, M.J., Wilk, A.J., Darby, C., Zager, M., et al. (2021). Integrated analysis of multimodal single-cell data. Cell *184*, 3573–3587.e3529. https://doi.org/10.1016/j.cell.2021.04.048.
61. Germain, P.-L., Lun, A., Macnair, W., and Robinson, M.D. (2021). Doublet identification in single-cell sequencing data using scDblFinder. F1000Research *10*, 979. https://doi.org/10.12688/f1000research.73600.1.
62. Aibar, S., González-Blas, C.B., Moerman, T., Huynh-Thu, V.A., Imrichova, H., Hulselmans, G., Rambow, F., Marine, J.-C., Geurts, P., Aerts, J., et al. (2017). SCENIC: single-cell regulatory network inference and clustering. Nat. Methods *14*, 1083–1086. https://doi.org/10.1038/nmeth.4463.
63. Subramanian, A., Tamayo, P., Mootha, V.K., Mukherjee, S., Ebert, B.L., Gillette, M.A., Paulovich, A., Pomeroy, S.L., Golub, T.R., Lander, E.S., and Mesirov, J.P. (2005). Gene set enrichment analysis: a knowledge-based approach for interpreting genome-wide expression profiles. Proc. Natl. Acad. Sci. USA *102*, 15545–15550. https://doi.org/10.1073/pnas.0506580102.
64. Wang, J.Y., and Doudna, J.A. (2023). CRISPR technology: A decade of genome editing is only the beginning. Science *379*, eadd8643. https://doi.org/10.1126/science.add8643.
65. Zhou, Y., Zhou, B., Pache, L., Chang, M., Khodabakhshi, A.H., Tanaseichuk, O., Benner, C., and Chanda, S.K. (2019). Metascape provides a biologist-oriented resource for the analysis of systems-level datasets. Nat. Commun. *10*, 1523. https://doi.org/10.1038/s41467-019-09234-6.
66. Andrews, N.C., and Faller, D.V. (1991). A rapid micrqpreparation technique for extraction of DNA-binding proteins from limiting numbers of mammalian cells. Nucleic Acids Res. *19*, 2499. https://doi.org/10.1093/nar/19.9.2499.
67. Detre, S., Jotti, G.S., and Dowsett, M. (1995). A quickscore method for immunohistochemical semiquantitation: validation for oestrogen receptor in breast carcinomas. J. Clin. Pathol. *48*, 876. https://doi.org/10.1136/jcp.48.9.876.
68. Liberzon, A., Birger, C., Thorvaldsdóttir, H., Ghandi, M., Mesirov, J.P., and Tamayo, P. (2015). The Molecular Signatures Database Hallmark Gene Set Collection. Cell Syst. *1*, 417–425. https://doi.org/10.1016/j.cels.2015.12.004.
69. Wu, T., Hu, E., Xu, S., Chen, M., Guo, P., Dai, Z., Feng, T., Zhou, L., Tang, W., Zhan, L., et al. (2021). clusterProfiler 4.0: A universal enrichment tool for interpreting omics data. Innovation *2*, 100141. https://doi.org/10.1016/j.xinn.2021.100141.

Please cite this article in press as: Guo et al., BRD9 inhibition overcomes oncolytic virus therapy resistance in glioblastoma, Cell Reports Medicine (2025), https://doi.org/10.1016/j.xcrm.2025.102258

STAR★METHODS

KEY RESOURCES TABLE

REAGENT or RESOURCE	SOURCE	IDENTIFIER
Antibodies		
Rabbit monoclonal anti-BRD9 antibody	Abcam	Cat# ab259839; RRID: N/A
Rabbit monoclonal anti-BRD9 antibody	Active motif	Cat# AM91413; RRID: AB_3216310
Rabbit polyclonal anti-BRD9 antibody	Active motif	Cat# AM65705; RRID: AB_3216381
Rabbit monoclonal anti-RELA antibody	Cell Signaling Technology	Cat# 8242; RRID: AB_10859369
Rabbit polyclonal anti-PCNA antibody	Proteintech	Cat# 10205-2-AP; RRID: AB_2160330
Mouse monoclonal anti- Calreticulin antibody	R&D	Cat# MAB38981; RRID: AB_2923351
Mouse monoclonal anti-GAPDH antibody	Proteintech	Cat# 60004-1-Ig; RRID: AB_2107436
Rabbit polyclonal anti-HSV1 antibody	Abcam	Cat# ab9533; RRID: AB_307320
Normal rabbit IgG antibody	Cell Signaling Technology	Cat# 2729S; RRID: AB_1031062
Rat monoclonal Pacific blue conjugated anti-CD45	Biolegend	Cat# 103126; RRID: AB_493536
Rat monoclonal APC conjugated anti-CD3	Biolegend	Cat# 100312; RRID: AB_312677
Rat monoclonal PE-Cy7 conjugated anti-CD4	Biolegend	Cat# 100421; RRID: AB_312706
Rat monoclonal PE conjugated anti-CD8	Biolegend	Cat# 100708; RRID: AB_312747
Rat monoclonal BV510 conjugated anti-CD69	Biolegend	Cat# 104531; RRID: AB_2562326
Rat monoclonal FITC conjugated anti-GranzymeB	Biolegend	Cat# 515403; RRID: AB_2114575
Rat monoclonal AF700 conjugated anti-CD11b	Biolegend	Cat# 101222; RRID: AB_493705
Rat monoclonal PE conjugated anti-F4/80	Biolegend	Cat# 157304; RRID: AB_2832547
Rat monoclonal PE-Cy5 conjugated anti-CD11c	Biolegend	Cat# 117316; RRID: AB_493566
Rat monoclonal Percp/Cy5.5 conjugated anti-I-A/I-E	Biolegend	Cat# 107626; RRID: AB_2191071
Rat monoclonal PE/Cyanine5 conjugated anti-CD44	Biolegend	Cat# 103009; RRID: AB_312960
Rat monoclonal Brilliant Violet 510 conjugated anti-CD62L	Biolegend	Cat# 104441; RRID: AB_2561537
Mouse monoclonal PE conjugated anti-XCR1	Biolegend	Cat# 148203; RRID: AB_2563842
Rat monoclonal APC conjugated anti-CD172a	Biolegend	Cat# 144013; RRID: AB_2564060
Rat monoclonal APC conjugated anti-P2RY12	Biolegend	Cat# 848005; RRID: AB_2721468
Rat monoclonal Biotin conjugated anti-CD25	Biolegend	Cat# 102004; RRID: AB_312853
Rat monoclonal PE conjugated anti-H-2	Biolegend	Cat# 125505; RRID: AB_1227706
TruStain FcX (anti-mouse CD16/32)	Biolegend	Cat# 101320; RRID: AB_1574975
Rat monoclonal InVivoPlus anti-PD1	BioXcell	Cat# BE0146; RRID: AB_10949053
Rat monoclonal InVivoPlus anti-CTLA4	BioXcell	Cat# BE0131; RRID: AB_10950184
Rat monoclonal InVivoMAb anti-CD8β	BioXcell	Cat# BE0223; RRID: AB_2687706
Anti-Mouse IgG, HRP-linked	Cell Signaling Technology	Cat# 7076; RRID: AB_330924
Anti-Rabbit IgG, HRP-linked	Cell Signaling Technology	Cat# 7074; RRID: AB_2099233
Anti-Mouse IgG (H + L) Secondary antibody, APC	Thermo Fisher	Cat# A865; RRID: AB_141364
Anti-Mouse IgG Secondary antibody, Alexa Fluor 488	Thermo Fisher	Cat# A21202; RRID: AB_141607
M280 Sheep anti-rabbit IgG Dynabeads	Thermo Fisher	Cat# 11203D; RRID: AB_2783009
CD45 microbeads	Miltenyi Biotech	Cat# 130-052-301; RRID: AB_2877061
Bacterial and virus strains		
Stabl3	AlpaLifeBio	Cat# KTSM110L
Endura electrocompetent cells	Lucigen	Cat# 60242-2
oHSV1	This study	N/A
HSV1-GFP	This study	N/A
HSV1-K26GFP	This study	N/A

(*Continued on next page*)

Please cite this article in press as: Guo et al., BRD9 inhibition overcomes oncolytic virus therapy resistance in glioblastoma, Cell Reports Medicine (2025), https://doi.org/10.1016/j.xcrm.2025.102258

Continued

REAGENT or RESOURCE	SOURCE	IDENTIFIER
Chemicals, peptides, and recombinant proteins		
Fixable Viability Dye eFlour 780	eBioscience	Cat# 65-0865-18
Dulbecco's modified Eagle's medium	Gibco	Cat# C11995500CP
RPMI 1640 mediun	Gibco	Cat# C22400500CP
Fetal bovine serum	Gibco	Cat# 10099-141C
Fetal bovine serum	CellMax	Cat# SA201.02
Penicillin/streptomycin supplement	Biosharp	Cat# P1400
GlutaMax supplement	Gibco	Cat# 35050-061
Neurobasal-A Medium without phenol red	Gibco	Cat# 12349-015
B-27 supplement	Gibco	Cat# 12587-010
L- glutamine	Gibco	Cat# A2916801
β-mercaptoethanol	Gibco	Cat# 31350010
Recombinant human EGF	R&D System	Cat# 236-EG
Recombinant human FGF	R&D System	Cat# 4114-TC
Recombinant mouse GM-CSF	Novoprotein	Cat# CK02
InVivoMAb recombinant Flt-3L-Ig (hum/hum)	BioXcell	Cat# BE0098
NLS-Cas9	GenScript	Cat# Z03702
Sodium Pyruvate	Gibco	Cat# 11360-070
Puromycin	InvivoGen	Cat# ant-pr-1
Blasticidin	Beyotime	Cat# ST018
Polyethyleneimine transfection reagent	Polyscience	Cat# 23966-1
Carboxymethlcellulose sodium	Solarbio	Cat# 8621
Retinoic acid	Sigma	Cat# R2625
TRIzol reagent	Thermo Fisher	Cat# 15596018
cDNA using NovoScript Plus All-in-one 1st Strand cDNA Synthesis Supermix	Novoprotein	Cat# E047
NovoStart SYBR qPCR SuperMix Plus	Novoprotein	Cat# E096
RIPA buffer	Beyotime	Cat# P0013C
Protease Inhibitor Cocktail	Roche	Cat# 4693132001
Bradford Protein assay	Beyotime	Cat# P0006C
SDS–PAGE Plus Sample Buffer	Genstar	Cat# E151-10
PVDF Tansfer Membranes	Merck	Cat# IPVH00010
LumiQ ECL reagent	Share-bio	Cat# SB-WB012
Rneasy Plus Animal RNA isolation kit	Beyotime	Cat# R0032
IBRD9	Selleck	Cat# S7835
SC75741	MCE	Cat# HY-10496
DMSO	Sigma	Cat# D-2850
Corn oil	Sigma	Cat# C8267
Fixation buffer	Biolegend	Cat# 420801
Intracellular staining buffer	Biolegend	Cat# 421002
2.5% horse serum	Vector Laboratories	Cat# MP-7401-50
ImmPRESS HRP Horse anti-Rabbit IgG Polymer detection kit	Vector Laboratories	Cat# MP-7401-50
DAB staining	ZSGB-BIO	Cat# ZLI-9017
Neutral balsam	Solarbio	Cat# G8590
Papin dissociation system	Worthington Biochemical	Cat# LK003153
RBC lysis buffer	Leagene	Cat# CS0001
Leukocyte Activation Cocktail, with BD GolgiPlug	BD	Cat# 550583

(*Continued on next page*)

Please cite this article in press as: Guo et al., BRD9 inhibition overcomes oncolytic virus therapy resistance in glioblastoma, Cell Reports Medicine (2025), https://doi.org/10.1016/j.xcrm.2025.102258

Continued

REAGENT or RESOURCE	SOURCE	IDENTIFIER
Critical commercial assays		
STEMdiff SMADi Neural Induction Kit	STEMCELL	Cat# 08581
STEMdif Cerebral Organoid Kit	STEMCELL	Cat# 08570
CellTiter-Glo Luminescent Assay	Promega	Cat# G7572
ATP assay kit	Beyotime	Cat# S0026
Human HMGB1 ELISA kit	Solarbio	Cat# SEKH-0409
Mouse HMGB1 ELISA kit	Solarbio	Cat# SEKM-0145
Annexin V-FITC and PI cell apoptosis assay	Yeasen	Cat# 40302ES60
TaKaRa MiniBEST Viral RNA/DNA Extraction Kit	TaKaRa	Cat# 9766
EasySep mouse T cell isolation Kit	STEMCELL	Cat# 19851A
CellTrace Violet Cell Proliferation Kits	Thermo Fisher	Cat# C34557
VAHTS Universal V8 RNA-seq Library Prep Kit for Illumina	Vanzyme	Cat# NR605-01
ChIP-IT High Sensitivity Kit	Active motif	Cat# 53040
NEBNext Ultra DNA Library Prep Kit for Illumina	NEB	Cat# E7645L
Chromium Next GEM Single-Cell 3′ Reagent Kit v3.1	10x Genomics	Cat# PN-1000121
Qubit High Sensitivity DNA assay	Thermo Fisher	Cat# Q33230
Deposited data		
Bulk RNA-seq data	This study	PRJNA1066491
BRD9 ChIP-seq data	This study	GEO: GSE260886
scRNA-seq data	This study	PRJNA1066491
RELA ChIP-seq data	Raju et al.[48]	GSM2394420
Experimental models: Cell lines		
HEK293T	ATCC	Cat# CRL-3216; RRID: CVCL_0063
$CT2A^{Nectin1}$	This study	N/A
$GL261^{Nectin1}$	This study	N/A
Vero	Procell	Cat# CL-0242; RRID: N/A
MGG4	Hiroaki Wakimoto	N/A
GSC3264	Hiroaki Wakimoto	N/A
BNI21	This study	N/A
ENSA	Jeremy Rich	N/A
hNP1	Jeremy Rich	N/A
iPSCs	ZQXZbio	Cat# DF-GMP-ZB11ALD-G-QX-22
H1	Kai Lei	N/A
Experimental models: Organisms/strains		
Mice: C57BL/6J	Jackson Laboratory	Cat# 000664; RRID: IMSR_JAX:000664
Mice: NOD.Cg-Prkdcscid Il2rgtm1Wjl/SzJ	Jackson Laboratory	Cat# 005557; RRID: IMSR_JAX:005557
Mice: C57BL/6-Tg(TcraTcrb)1100Mjb/J	Jackson Laboratory	Cat# 003831; RRID: IMSR_JAX:003831
Oligonucleotides		
Primers for Quantitative real-time PCR, see Table S1	This paper	N/A
Primers for ChIP-qPCR, see Table S1	This paper	N/A
SgRNA for individual genes knockout, see Table S2	This paper	N/A
Recombinant DNA		
CRISPR Mouse Knockout Pooled Library (Bire)	Addgene	Cat# 73632; RRID: Addgene_73632
Plasmid: psPAX2	Addgene	Cat# 12260; RRID: Addgene_12260
Plasmid: pMD2.G	Addgene	Cat# 12259; RRID: Addgene_12259
Plasmid: lentiCRISPR v2	Addgene	Cat# 52961; RRID: Addgene_52961
Plasmids: pLenti-mus Nectin1	This study	N/A
Plasmid: PLVX-OVA-P2A-zsGreen	This study	N/A

(*Continued on next page*)

Please cite this article in press as: Guo et al., BRD9 inhibition overcomes oncolytic virus therapy resistance in glioblastoma, Cell Reports Medicine (2025), https://doi.org/10.1016/j.xcrm.2025.102258

Continued

REAGENT or RESOURCE	SOURCE	IDENTIFIER
Software and algorithms		
GraphPad Prism v8.4.3	GraphPad	https://www.graphpad.com/
FlowJo software v10.4	FlowJo	https://www.flowjo.cn/
HISAT2 v2.2.1	Kim et al.[49]	http://daehwankimlab.github.io/hisat2/
FeatureCount v2.0.3	Liao et al.[50]	https://subread.sourceforge.net/featureCounts.html
DESeq2 v1.38.3	Love et al.[51]	https://bioconductor.org/packages/release/bioc/html/DESeq2.html
Fastp v0.23.2	Chen et al.[52]	https://github.com/OpenGene/fastp
Bowtie2 v2.4.5	Langmead et al.[53]	https://bowtie-bio.sourceforge.net/bowtie2/index.shtml
SAMtools v1.16.1	Danecek et al.[54]	https://github.com/samtools/samtools
MarkDuplicates v2.27.4	MarkDuplicates	https://gatk.broadinstitute.org/hc/en-us/articles/360037052812-MarkDuplicates-Picard
MACS2 v2.2.7.1	Zhang et al.[55]	https://github.com/macs3-project
ChIPSeeker v1.34.1	Yu et al.[56]	https://bioconductor.org/packages/release/bioc/html/ChIPseeker.html
DeepTools v3.5.2	Ramírez et al.[57]	https://github.com/deeptools/deepTools
IGV v2.13.1	Thorvaldsdottir et al.[58]	https://igv.org/
Cell Ranger v7.1.0	10x Genomics	https://github.com/10XGenomics/cellranger
CellBender v0.3.0	Fleming et al.[59]	https://github.com/broadinstitute/CellBender
Seurat v4.3.0	Hao et al.[60]	https://satijalab.org/seurat/
scDblFinder v1.14.0	Germain et al.[61]	https://github.com/plger/scDblFinder
AUCell v1.22.0	Aibar et al.[62]	https://github.com/aertslab/AUCell
Msigdbr v7.5.1	Aravind et al.[63]	https://github.com/igordot/msigdbr
Trim Galore software v0.6.10	Trim Galore software	https://github.com/FelixKrueger/TrimGalore
MAGeCK software v0.5.0	Wang et al.[64]	https://github.com/liulab-dfci/MAGeCK
Metascape webtool	Zhou et al.[65]	https://metascape.org/gp/index.html
BAGEL2	Hart et al.[18]	https://github.com/hart-lab/bagel
R studio v4.0.3	R studio	https://posit.co/download/rstudio-desktop/

EXPERIMENT MODEL AND STUDY PARTICIPANT DETAILS

Cell lines and cell culture

HEK293T cells were acquired from the American Type Culture Collection (ATCC, #CRL-3216) and cultivated in Dulbecco's modified Eagle's medium (DMEM; Gibco, #C11995500CP) supplemented with 10% fetal bovine serum (Gibco, #10099-141C), 1% penicillin/streptomycin (Biosharp, #P1400), and 1% GlutaMax Supplement (Gibco, #35050-061). The mouse glioma cell lines CT2A^{Nectin1} and GL261^{Nectin1} were cultured in Dulbecco's modified Eagle medium (Gibco, #C11995500CP) supplemented with 10% fetal bovine serum (CellMax, #SA201.02) and 1% penicillin/streptomycin (Biosharp, #P1400) at 37°C in an incubator with 5% CO_2. The Vero cells were maintained under the same conditions as the mouse glioma cells. The human glioblastoma stem cell line (MGG4, GSC3264 and BNI21) and normal neural progenitor cells (ENSA and hNP1) were cultured in Neurobasal-A Medium without phenol red (Gibco, #12349-015) supplemented with B-27 supplement (Gibco, #12587-010), 20 ng/mL recombinant human EGF protein (R&D, #236-EG), 20 ng/mL recombinant human FGF basic protein (R&D, #4114-TC), 1% penicillin/streptomycin (Biosharp, #P1400), 1% sodium pyruvate (Gibco, #11360-070), and 1% GlutaMax supplement (Gibco, #35050-061) at 37°C in an incubator with 5% CO_2.

Mice

C57BL/6J mice (The Jackson Laboratory, #000664) and NOD.Cg-Prkdcscid Il2rgtm1Wjl/SzJ mice (NSG, The Jackson Laboratory, #005557), aged 6–8 weeks, were obtained from the Laboratory Animal Resource Center (LARC) of Westlake University. C57BL/6-Tg (TcraTcrb)1100Mjb/J mice were kindly gifted from Dr. Lianjun Zhang (Suzhou Institute of Systems Medicine). All animal experiments conducted in this study were approved by the Institutional Animal Care and Use Committee (IACUC) of Westlake University and adhered to all relevant ethical regulations (permission numbers: 19-028-2-XQ). The mice were housed in specific pathogen-free facilities at the LARC of Westlake University with a 12-h light–dark cycle and an ambient temperature of 20°C–25°C.

CellPress
OPEN ACCESS

Cell Reports Medicine
Article

Tumor models and *in vivo* experiments

In the Brd9-deficient tumor mice models, C57BL/6J mice were intracranially injected with 2×10^4 Brd9-deficient or control CT2A^{Nectin1} cells (or GL261^{Nectin1} cells) using an animal stereotactic frame (RWD Instruments) and a 26-gauge microliter syringe (Hamilton Company). For the survival experiments, 3 days after tumor injection (or 7 days after tumor injection), the mice were randomly divided into groups that received intracranial injections (at the same stereotactic coordinates) of oHSV1 (6×10^5 PFU in day3 or 2×10^6 PFU in day7) or PBS. Mice were then monitored daily and euthanized when they displayed signs of becoming moribund or neurological impairment, and their survival time was recorded. For the immune cell infiltration experiments and virus replication experiments, 17 days after tumor implantation, the mice were randomly divided into groups that received intracranial injections of oHSV1 (6×10^5 PFU) or PBS. Mice were euthanized 2 days post-treatment to assess immune cell infiltration in tumors via flow cytometry and single-cell RNA sequencing, and to evaluate viral replication using anti-HSV1 immunohistochemistry staining and quantitative real-time PCR.

In the BRD9-deficient tumor mice model, NSG mice were intracranially injected 1×10^4 BRD9-deficient or control MGG4 cells. For the survival experiments, 7 days after tumor injection, the mice were randomly divided into groups that received intracranial injections (at the same stereotactic coordinates) of oHSV1 (1×10^6 PFU) or PBS. Mice were then monitored daily and euthanized when they displayed signs of becoming moribund or neurological impairment, and their survival time was recorded.

In the IBRD9-treated tumor mice models, C57BL/6J mice were intracranially injected with 2×10^4 CT2A^{Nectin1} (or GL261^{Nectin1}) cells. For survival experiments, the mice were randomly divided into 8 groups: Group 1, mock group; Group 2, oHSV1 treatment group; Group 3, IBRD9 treatment group; Group 4, combination treatment of IBRD9 and oHSV1 group; Group 5, immune checkpoint blockade (ICB) treatment group; Group 6, combination treatment of ICB and oHSV1 group; Group 7, combination treatment of IBRD9 and ICB group; and Group 8, combination treatment of IBRD9, ICB and oHSV1. IBRD9 (Selleck, #S7835) was dissolved in DMSO (Sigma, #D-2850), diluted in corn oil at 2mg/mL and intraperitoneally administered to mice at the concentration of 16 mg/kg on days 2–4 after tumor injection. The anti-mouse PD1 antibody (Bioxcell, #BE0146) and anti-mouse CTLA4 antibody (Bioxcell, #BE0131) were used for ICB treatment and diluted in PBS before intraperitoneal injection at the concentration of 10 mg/kg on days 4, 7, and 10. A total of 6×10^5 PFU of oHSV1 was used for intracranial injection on day 3. The mice were euthanized when they became moribund or displayed neurological impairment, and the survival time was recorded. For the immune cell infiltration experiment, the tumor-bearing mice were randomly divided into 4 groups: Group 1, mock group; Group 2, oHSV1 group; Group 3, IBRD9 group; and Group 4, combination treatment of IBRD9 and oHSV1 treatment group. IBRD9 was administered on days 16–18 after the tumor injection. A total of 6×10^5 PFU of oHSV1 was used for intracranial injection on day 17. Mice were euthanized on day 19 to evaluate immune cell tumor infiltration using flow cytometry as described below.

For CD8$^+$ T cell depletion experiment, C57BL/6J mice were intracranially injected with 2×10^4 Brd9-deficient or control CT2A^{Nectin1} cells. For survival studies, 3 days after tumor injection, the mice were randomly divided into groups that received intracranial injections (at the same stereotactic coordinates) of oHSV1 (6×10^5 PFU) or PBS. Then the mice were randomly divided into 3 groups: Group 1, mock group; Group 2, IgG treatment group and Group 3, anti-mouse CD8 antibody treatment group. The anti-mouse CD8 antibody (Bioxcell, #BE0223) was used for CD8$^+$ T cell depletion *in vivo* and diluted in PBS before intraperitoneal injection at the concentration of 8 mg/kg on day 2, 6, and 10. Mice were then monitored daily and euthanized when they displayed signs of becoming moribund or neurological impairment, and their survival time was recorded.

For the tumor rechallenge experiments, long-term survivor mice from the triple combination therapy experiment were intracranially injected with 2×10^4 CT2A^{Nectin1} (or GL261^{Nectin1}) cells 60 days later after the initial tumor injection. Age-matched control C57BL/6J mice were also intracranially injected with 2×10^4 CT2A^{Nectin1} (or GL261^{Nectin1}) cells. Mice were then monitored daily and euthanized when they displayed signs of becoming moribund or neurological impairment, and their survival time was recorded.

For the safety assessment of oHSV1, C57BL/6J mice were intracranially injected with oHSV1 (6×10^5 PFU) or PBS. Animals were monitored daily for clinical signs, with body weight recorded every 3 days, and survival times were tracked. On day 18 post-injection, major organs (brain, heart, liver, spleen, lung, kidney, intestine, and colon) were collected and subjected to hematoxylin and eosin staining to evaluate viral safety in mouse tissues.

METHOD DETAILS

DNA clones and plasmids

The sgRNA sequences for the target genes were cloned and inserted into the lentiCRISPRV2 vector (Addgene, #52961).

CRISPR-mediated pooled library lentivirus production

The CRISPR Mouse Knockout Pooled Library (Brie) (Addgene, #73632), which comprises 78,637 sgRNAs targeting 19,674 genes, was utilized for the generation of lentivirus. Cotransfection of the library plasmid, psPAX plasmid (Addgene, #12269), and pMD2. G plasmid (Addgene, #12259) was carried out in HEK293T cells using polyethyleneimine transfection reagent (1 mg/mL; Polyscience, #23966-1) following the manufacturer's protocol. The library plasmid (18 μg), psPAX plasmid (12 μg), and pMD2. G plasmids (6 μg) were combined and transfected into HEK293T cells in 15-cm plates. After transfection, the culture medium was removed 12 h later and replaced with fresh medium. After 48 h, the culture medium was collected and subjected to ultracentrifugation at 70,000 × g for 2 h at 4°C (Beckman Coulter). The resulting pellets were resuspended in DMEM and stored at −80°C.

Please cite this article in press as: Guo et al., BRD9 inhibition overcomes oncolytic virus therapy resistance in glioblastoma, Cell Reports Medicine (2025), https://doi.org/10.1016/j.xcrm.2025.102258

CellPress
OPEN ACCESS

CRISPR screening

The CRISPR Mouse Knockout library lentivirus was utilized to transduce the CT2A^{Nectin1} cells. Following the 12-h infection period, the cells were allowed to recover for 24 h and then selected with puromycin (1 μg/mL, InvivoGen, #ant-pr-1) for 4 days. Cells transduced with the library were divided equally into two groups for screening: the oHSV1 treatment group and the control group. The cells were treated with oHSV1 at a multiplicity of infection (MOI) of 0.5 for 48 h and then washed with PBS. Genomic DNA isolated from the remaining cells treated with oHSV1, as well as from the cells in the control group, was used to prepare the library for next-generation sequencing.

Analysis of CRISPR screening data

FASTQ files were first processed by Trim Galore software (v0.6.10) to remove any unnecessary genomic sequences. The resulting trimmed FASTQ files were then subjected to analysis using MAGeCK software (v0.5.9),[17] allowing for the quantification of sgRNA read counts. This analysis employed the maximum-likelihood estimation (MLE) algorithm provided by MAGeCK, which facilitated the identification of sgRNAs and genes that exhibited significant enrichment or depletion in the oHSV1-treated samples compared with the control samples. The genes that were not involved in cell proliferation were subjected to Gene Ontology analysis using Metascape webtool.[65] The quality control of CRISPR screening data were analyzed by Bayesian Analysis of Gene Essentiality 2 (BAGEL2) approach.[18,19]

Oncolytic HSV1 and HSV1-GFP production and plaque assay

Oncolytic HSV1 (oHSV1) was generated by inserting miR124T into the ICP34.5 promoter region and inserting human GM-CSF cDNA into the same promoter region. oHSV1, HSV1-K26GFP and HSV1-GFP were subsequently propagated in Vero cells by infecting them with the virus at 0.05 MOI. The supernatant was collected and subsequently ultracentrifuged at 20,000 × g for 5 h at 4°C using an ultracentrifuge (Beckman Coulter). The resulting viral pellets were resuspended in PBS. To determine the virus titers, a plaque formation assay was performed. Briefly, Vero cells (2×10^5/well) were seeded into a 24-well plate and cultured overnight. The monolayer of Vero cells was infected with a gradient-diluted viral solution. 3h after infection, the viral medium was removed, and the cells were washed three times with PBS. Overlay medium containing 1% carboxymethylcellulose sodium (Solarbio, #8621) was added, and the plates were then incubated at 37°C for 48–60 h until plaques were visible under a light microscope. The carboxymethylcellulose sodium medium was removed, and the cells were fixed with 4% paraformaldehyde at room temperature. After washing three times with PBS, the cells were stained with a 0.1% crystal violet solution (Solarbio, #G1063), and the number of plaques was counted. The plaque-forming units (PFUs)/mL were calculated using the following formula: number of plaques/(dilution ratio × volume of viral medium).

Neuronal differentiation and cerebral organoid induction

For neuronal differentiation, induced pluripotent stem cells (iPSCs) were acquired from ZQXZbio (ZQXZbio, #DF-GMP-ZB11ALD-G-QX-22) and firstly induced into neural progenitor cells (NPCs) using the STEMdiff SMADi Neural Induction Kit (STEMCELL, #08581) following the manufacturer's instructions. Then, the NPCs were differentiated into neurons after treatment with 1 μM retinoic acid (Sigma, #R2625) for 14 days.

For cerebral organoid induction, human embryonic stem cells (hESCs) H1 cells were kindly provided by Dr. Kai Lei (Westlake University). H1 cells were induced into cerebral organoids using the STEMdiff Cerebral Organoid Kit (STEMCELL, #08570) following the manufacturer's instructions.

Dose–response cytotoxicity

A total of 1×10^4 cells were seeded in 96-well white plates (NEST, #701001) in triplicate. The cells were then infected with oHSV1 at 0.2 and 0.5 MOIs for 6 h. After infection, the viral medium was removed and replaced with normal culture medium. The plates were then incubated for 24 h, after which cell viability was measured using the CellTiter-Glo Luminescent Assay (Promega, #G7572). Luminescence readings were obtained using a Varioskan LUX microplate reader (Thermo Fisher Scientific) with a gain setting of 100 ms. The mock-treated cell readings were used to indicate 100% survival.

Cell proliferation and cell apoptosis assays

Cell proliferation was evaluated using the CellTiter-Glo Luminescent Cell Viability Assay (Promega, #G7572) following the manufacturer's instructions. Luminescence readings were obtained using a Varioskan LUX microplate reader (Thermo Fisher Scientific). Cell apoptosis was assessed by the Cytoflex flow cytometer (Beckman Coulter) after performing double staining with Annexin V-FITC and PI (Yeasen, #40302ES60).

Calreticulin (CRT) exposure assay

oHSV1 Infected cells and control cells were stained with the anti-calreticulin antibody (R&D, # MAB38981-SP) and then stained with Goat anti-Mouse IgG (H + L) Cross-Adsorbed Secondary Antibody, APC (Thermo Fisher Scientific, #A865). The data was assessed by the Cytoflex flow cytometer (Beckman Coulter).

Please cite this article in press as: Guo et al., BRD9 inhibition overcomes oncolytic virus therapy resistance in glioblastoma, Cell Reports Medicine (2025), https://doi.org/10.1016/j.xcrm.2025.102258

Extracellular ATP detection assay

The supernatants of oHSV1 infected cells and control cells were collected. Extracellular ATP in the supernatants was measured with the ATP assay kit (Beyotime, #S0026) following the manufacturer's instructions. Luminescence readings were obtained using a Varioskan LUX microplate reader (Thermo Fisher Scientific).

ELISA

The supernatants of oHSV1 infected cells and control cells were collected. Human HMGB1 in the supernatants was measured with the Human HMGB1 ELISA kit (Solarbio, #SEKH-0409) following the manufacturer's instructions. Mouse HMGB1 in the supernatants was measured with the Mouse HMGB1 ELISA kit (Solarbio, #SEKM-0145) following the manufacturer's instructions.

Viral binding assay

A total of 5×10^5 BRD9-deficient and control MGG4 and CT2A^{Nectin1} cells were incubated with 5×10^6 PFU of HSV1-K26GFP for 45 min on ice and washed 3 times with PBS to remove the unbound virus. The samples were analyzed by the Cytoflex flow cytometer (Beckman Coulter).

Viral entry kinetics assay

A total of 5×10^4 BRD9-deficient and control MGG4 and CT2A^{Nectin1} cells per cell were seeded on 48-well plates. The cells were grown overnight, after which the culture media was replaced with fresh media containing 5×10^3 PFU of HSV1-GFP. The infection media were removed at 5, 10, 20, 40, 60, 90, 120, 180, 240, 300 or 360 min after infection. The cells were washed twice with PBS, after which overlay medium supplemented with 1% carboxymethylcellulose sodium (Solarbio, #8621) was added to cover the cells. 48 h after infection, the cells were harvested for flow cytometry analysis. Viral entry kinetics curves were established by relating the relative percentage of GFP-positive cells to the viral incubation time to evaluate the viral entry speed.[36]

Quantification of viral load

To quantify viral DNA in mouse tumors, tumor samples were collected and viral DNA was extracted using the TaKaRa MiniBEST Viral RNA/DNA Extraction Kit (TaKaRa, #9766) according to the manufacturer's instructions. Viral DNA abundance was then quantified via quantitative real-time PCR. The primers used for PCR amplification are described in Table S1.

Quantitative real-time PCR

Total RNA was extracted using TRIzol Reagent (Thermo Fisher Scientific, #15596018) and reverse transcribed into cDNA using NovoScript Plus All-in-one 1st Strand cDNA Synthesis Supermix (Novoprotein, #E047) according to the manufacturer's protocol. Quantitative real-time PCR was performed using NovoStart SYBR qPCR SuperMix Plus (Novoprotein, #E096) in 96-well plates, and the data were read with a CFX Connect Real-Time System (Bio-Rad). For qPCR data analysis, we used the typical $\Delta\Delta$CT method to calculate these genes expression that were normalized to the housekeeping gene GAPDH. The primers used for PCR amplification are described in Table S1.

Western blotting

The cells were lysed using RIPA buffer (Beyotime, #P0013C) supplemented with Protease Inhibitor Cocktail (Roche, #4693132001), and the protein concentrations were determined using the Detergent Compatible Bradford Protein Assay Kit (Beyotime, #P0006C). For western blotting, equal amounts of protein were denatured by heating in the presence of SDS–PAGE Plus Sample Buffer (GenStar, #E151-10). The proteins were then separated on 8% SDS–PAGE gels and transferred to PVDF Transfer Membranes (Merck, #IPVH00010). The antibodiesare listed in the key resources table. Protein detection was performed using the LumiQ ECL reagent (Share-bio, SB-WB012) and the ChemiDoc XRS+ Imaging System (Bio-Rad).

RNA-seq library preparation and analysis

oHSV1-treated BRD9-deficient and control MGG4 cells were obtained and processed to construct RNA-seq libraries. Total RNA was extracted using a RNeasy Plus Animal RNA Isolation Kit (Beyotime, #R0032) following the manufacturer's instructions. RNA-seq libraries were prepared using the VAHTS Universal V8 RNA-seq Library Prep Kit for Illumina (Vazyme, # NR605-01) following the manufacturer's protocol. All of the libraries were sequenced using a NovaSeq 6000 sequencer (Illumina).

For RNA-seq analysis, the reads were aligned to the GRCh38 reference genome using HISAT2[49] (v2.2.1) with default parameters. The raw counts per gene were quantified using FeatureCount[50] (v2.0.3). Differential expression analysis was conducted using the DESeq2[51] (v1.38.3) R package. Differentially expressed genes were identified based on a Bonferroni adjusted p value less than 0.05 and a log2-fold change greater than 1.

Chromatin immunoprecipitation sequencing (ChIP-Seq) library preparation and analysis

BRD9-deficient and control MGG4 cells were collected and processed to generate ChIP-Seq libraries using the ChIP-IT High Sensitivity Kit (Active Motif, #53040). Briefly, 6×10^6 cells were cross-linked for 10 min with 1% formaldehyde at room temperature, and the reaction was subsequently quenched with 125 mmol/L glycine for 5 min. The fixed cells were homogenized for 30 strokes to lyse the

Please cite this article in press as: Guo et al., BRD9 inhibition overcomes oncolytic virus therapy resistance in glioblastoma, Cell Reports Medicine (2025), https://doi.org/10.1016/j.xcrm.2025.102258

cells, and the chromatin was fragmented via sonication with a Bioruptor Pico (Diagenode). The digested chromatin was incubated with 5 μg of BRD9 antibody (Active Motif, #91413) overnight at 4°C. The antibody-chromatin complexes were pulled down by incubation with Protein G agarose beads for 3 h at 4°C. The immunoprecipitated DNA was decrosslinked and purified following the manufacturer's instructions. Purified DNA was used for library generation using the NEBNext Ultra 2 DNA library Prep kit for illumina (NEB, #E7645S) according to the manufacturer's instructions. All of the libraries were sequenced on a NovaSeq 6000 sequencer (Illumina).

For ChIP-seq analysis, raw sequencing reads were trimmed using fastp[52] (v0.23.2) to remove the adapters and subsequently aligned to the GRCh38 human genome using Bowtie2[53] (v2.4.5). All reads with a MAPQ <30 or mapping to mitochondria were removed using SAMtools[54] (v1.16.1). PCR duplicates were removed using PicardTools MarkDuplicates (v2.27.4). Peaks were identified with MACS2[55] (v2.2.7.1) with a *p* value threshold of 0.001. The peaks were annotated by ChIPSeeker[56] (v1.34.1) R package. Normalized BigWig files were generated by DeepTools[57] (v3.5.2), and the genome tracks were visualized in IGV.[58]

Chromatin immunoprecipitation quantitative real-time PCR (ChIP-qPCR)

BRD9-deficient and control MGG4 cells were collected and processed to generate ChIP-Seq libraries using the ChIP-IT High Sensitivity Kit (Active Motif, #53040). The immunoprecipitated DNA was decrosslinked and purified following the manufacturer's instructions. Quantitative real-time PCR was performed using NovoStart SYBR qPCR SuperMix Plus (Novoprotein, #E096) in 96-well plates, and the data were read with a CFX Connect Real-Time System (Bio-Rad). For qPCR data analysis, we used the typical percentage input method to calculate. The primers used for ChIP-qPCR amplification are described in Table S1.

Nuclear protein extraction and co-IP

Nuclear lysates were collected from MGG4 cells following a revised Dignam protocol.[66] A total of 1×10^7 cells were collected and suspended in Buffer A (10 mM HEPES pH = 7.9, 1.5 mM $MgCl_2$, 10 mM KCl) supplemented with 1 mM DTT and protease inhibitor cocktail (Roche, #4693132001). The cells were lysed by homogenization using a 21-gauge needle with 10 plunger pushes. Nuclei were centrifuged at 700 × g for 5 min at 4°C. The pellet was resuspended in Buffer C (20 mM HEPES pH = 7.9, 20% glycerol, 420 mM NaCl, 1.5 mM $MgCl_2$, 0.2 mM EDTA) supplemented with 1 mM DTT and Protease Inhibitor Cocktail (Roche, #4693132001). After 30 min of end−to-end rotation at 4°C, the sample was centrifuged at 18000 × g for 15 min at 4°C, after which the supernatant was collected. The nuclear lysate was diluted with two-thirds of the original volume of dilution buffer (50 mM Tris-HCl (pH = 8), 0.3% NP-40, 0.2 mM EDTA, and 1.5 mM $MgCl_2$). Protein concentrations were determined using the Detergent Compatible Bradford Protein Assay Kit (Beyotime, #P0006C) according to the manufacturer's instructions. For the co-IP reaction, 500 μg of nuclear lysates was incubated with 5 μg of BRD9 antibody (Active Motif, #65705) or normal rabbit IgG antibody (Cell Signaling, #2729S) overnight at 4°C with end-to-end rotation. Immunoprecipitated proteins were incubated with M280 Sheep Anti-Rabbit IgG Dynabeads (Thermo Fisher Scientific, #11203D) for 1 h at 4°C and washed 5 times with IP wash buffer (50 mM Tris, pH = 8; 150 mM NaCl; 1 mM EDTA; 10% glycerol; 0.5% Triton X-100). Proteins were eluted in SDS−PAGE Plus Sample Buffer (GenStar, #E151-10), boiled for 10 min and analyzed via western blotting.

Flow cytometry

Tumors were harvested, minced, and digested using the Papain Dissociation System (Worthington Biochemical, #LK003153) following the manufacturer's protocol. After digestion, the single cells were filtered through a 70-μm nylon cell strainer (NEST, #258368). The single-cell suspensions were incubated with TruStain FcX (anti-mouse CD16/32, 93, 1:400) in PBS. Fixable Viability Dye eFluor 780 (ThermoFisher Scientific, #65-0865-18) was used to differentiate between living and dying/dead cells. The surface staining at 4°C for 45 min and the intracellular staining was performed with fixation buffer (Biolegend, #420801) and intracellular staining buffer (Biolegend, #421002) according to the manufacturer's instructions. Cells were stained with the following anti-mouse antibodies at the indicated dilutions: CD45 (30-F11, 1:200), CD3 (145-2C11, 1:200), CD4 (GK1.5, 1:200), CD8 (53–6.7, 1:200), CD69 (H1.2F3, 1:200), Granzyme B (QA16A02, 1:200), CD11b (M1/70, 1:200), F4/80 (QA17A29, 1:200), CD11c (N418, 1:200), I-A/I-E (M5/114.152, 1:200), CD44 (IM7, 1:200) CD62L (MEL-14, 1:200), XCR1 (ZET, 1:200), CD172a (P84, 1:200) and P2RY12 (S16007D, 1:200) all purchased from Biolegend. Data acquisition was performed using the Aurora Cytometer (Cytek Biosciences). Data analysis was conducted using the FlowJo software (v10.4) (BD Biosciences).

Immunohistochemistry

To analyze *in vivo* oHSV1 infection in tumor cells, mice were implanted with either Brd9-deficient $CT2A^{Nectin1}$ cells or control $CT2A^{Nectin1}$ cells (2×10^4/mouse) on day 0. On day 17, the mice were intracranially injected with 6×10^5 PFU of oHSV1 or PBS. On day 19, the mice were euthanized, and their brains were isolated and fixed with 4% paraformaldehyde. The brains were then embedded in paraffin, and 8 μm sections were subjected to immunohistochemical staining. To prepare the sections for staining, the deparaffinized and dehydrated sections were boiled for 15 min in Tris/EDTA buffer (10mM Tris, 1 mM EDTA, 0.05% Tween 20, pH = 9.0), and incubated with 2.5% horse serum (Vector Laboratories, #MP-7401-50). Subsequently, the sections were incubated with an anti-HSV1 antibody (1:100; Abcam, #ab9533) for 1 h at room temperature, followed by incubation with an ImmPRESS HRP Horse Anti-Rabbit IgG Polymer Detection Kit for IHC (Vector Laboratories, #MP-7401-50). For DAB staining (ZAG-BIO, #ZLI-9017), sections were incubated with 50 μL of DAB solution (prepared by adding 20 μL of chromogen to 1 mL of DAB substrate) for 1 min, rinsed with water, counterstained with hematoxylin.

Please cite this article in press as: Guo et al., BRD9 inhibition overcomes oncolytic virus therapy resistance in glioblastoma, Cell Reports Medicine (2025), https://doi.org/10.1016/j.xcrm.2025.102258

To investigate the correlation between the therapeutic effects of oHSV1 and BRD9 expression, biopsy sections of liver cancer and pancreatic cancer tissues were obtained from patients participating in an oHSV1 clinical trial (NCT04806464) at The First Affiliated Hospital of Zhejiang University. These biopsy sections were collected with appropriate consent and in compliance with a protocol approved by the IRB. The sections were deparaffinized and boiled for 15 min in Tris/EDTA buffer, blocked with 5% horse serum (Vector Laboratories, #MP-7401-50), and then stained with an anti-BRD9 antibody (1:500; Abcam, #ab259839) for 1 h at room temperature. Afterward, the sections were incubated with an ImmPRESS HRP Horse Anti-Rabbit IgG Polymer Detection Kit for IHC (Vector Laboratories, #MP-7401-50) and subjected to DAB staining. The sections were counterstained with hematoxylin and mounted with neutral balsam (Solarbio, #G8590).

Immunohistochemistry and immunofluorescence were visualized using a Nikon Ni-E motorized fluorescence microscope. Cell counts were obtained from at least three random fields. For biopsy section statistics, the H-score method was used for immunohistochemical semiquantitation.[67]

Single-cell RNA-seq library preparation

Tumors were harvested, minced, and digested using the Papain Dissociation System (Worthington Biochemical, #LK003153) according to the manufacturer's protocol. Tumor-infiltrating leukocytes were isolated using CD45 microbeads (Miltenyi Biotech, #130-052-301) according to the manufacturer's protocol. The cells were counted, and approximately 7000 single cells were loaded onto a 10x Genomics Chromium (10x Genomics) to generate single-cell gel beads-in-emulsion (GEMs). Single-cell RNA libraries were generated using the Chromium Next GEM Single-Cell 3′ Reagent Kit v3.1 (10x Genomics, #PN-1000121). The libraries were quantified using the Qubit High Sensitivity DNA assay (Thermo Fisher Scientific, #Q33230), and the size distribution of the libraries was determined using the Fragment Analyzer-12/96 (Agilent). Finally, all the libraries were sequenced using a NovaSeq 6000 sequencer (Illumina).

Single-cell RNA-seq data analysis

For single-cell RNA-seq analysis, the raw sequencing data were processed against the mm10 mouse reference genome using Cell Ranger software (v7.1.0, 10× Genomics). Ambient RNA was removed using CellBender[59] (v0.3.0) with default parameters. The corrected expression matrix generated by CellBender was analyzed with the Seurat[60] (v4.3.0) R package for subsequent processing. The following criteria were applied to each sample to remove low-quality cells: a gene number between 500 and 8,000, a unique molecular identifier (UMI) count between 1,000 and 50,000, and a mitochondrial content <10%. Doublets were removed using the scDblFinder[61] (v1.14.0) R package. The cells that did not express Ptprc were removed. After filtering, a total of 9,179 cells remained. The filtered gene-count matrix was scaled and normalized for sequencing depth using Seurat's 'SCTransform' function (vars.to.regress = c("nCount_RNA"), vst.flavor = "v2"). The top 30 principal components were utilized for clustering and visualization. Finally, we obtained 14 clusters with a resolution = 0.2. Differentially expressed genes (DEGs) were identified by Seurat's 'FindAllMarkers' function with a Bonferroni adjusted *p* value less than 0.05 and a log2-fold change greater than 0.25. The reclustering procedures for T cells was similar to those described above.

Pathway enrichment analysis

Multiple gene sets (Hallmark, KEGG, Reactome, GOBP) were retrieved from The Molecular Signatures Database (MSigDB)[68] using msigdbr[63] (v7.5.1) (https://github.com/igordot/msigdbr/). The clusterProfiler[69] (v4.6) R package was used to perform pathway enrichment analysis and gene set enrichment analysis (GSEA). *p* values were adjusted using Benjamini–Hochberg FDR correction.

Bone marrow-derived conventional dendritic cells type 1 differentiation and culture

cDC1 were cultured with complete culture medium contains RPMI 1640 (Gibco, #C22400500CP) supplemented with 10% fetal bovine serum (Gibco, #10099-141C), 1% penicillin/streptomycin (Biosharp, #P1400), 2mM L-glutamine (Gibco, # A2916801), 50 μM β-mercaptoethanol (Gibco, # 31350010), 2 ng/mL recombinant mouse GM-CSF (Novoprotein, # CK02) and 200 ng/mL recombinant Flt-3L-Ig (BioXcell, # BE0098). The medium supplemented with 200 ng/mL Flt-3L-Ig was refreshed every 3 days. At day 12, all non-adherent and semi-adherent cells were collected in complete medium for cross presentation experiment.

CD25-negative OT-I T cells isolation

Spleen cells were isolated from OT-I transgenic mice, and CD25-negative OT-I T cells were subsequently purified using the EasySep Mouse T cell Isolation Kit (STEMCELL, #19851A). The isolation process was modified by supplementing the antibody cocktail with a CD25-biotin antibody (BioLegend, #102004), following the manufacturer's protocol.

Cross-presentation

The CT2A^{Nectin1} cells were infected with ovalbumin-P2A-zsGreen lentivirus to generate CT2A^{Nectin1}-OVA cells, which were subsequently sorted based on GFP fluorescence. To create β2m knockout CT2A^{Nectin1}-OVA cells (hereafter referred to as CT2A^{Nectin1}-OVA-B2m$^{-/-}$ cells), sgRNAs targeting β2m were combined with NLS-Cas9 (GenScript, #Z03702) at a ratio of 1:3 to form Cas9-sgRNA ribonucleoprotein (RNPs) complexes. These complexes were introduced into CT2A^{Nectin1}-OVA cells via nucleofection using the X-100 program on a 2b nucleofector system (Lonza). The H-2Kb/H-2Db negative CT2A^{Nectin1}-OVA cells were sorted by flow

cytometry, and the resulting β2m-KO CT2A^{Nectin1}-OVA cells were co-cultured with OT1 T cells to eliminate any residual β2m positive CT2A^{Nectin1}-OVA cells. Next, 2,000 IBRD9 pretreated CT2A^{Nectin1}-OVA-B2m$^{-/-}$ cells (1μm, 24h) or 2000 Brd9-deficient CT2A^{Nectin1}-OVA-B2m$^{-/-}$ were seeded into 96-well U-bottom plates. Subsequently, oHSV1 was added at a multiplicity of infection (MOI) of 0.2, and after 6 h, the cells were washed with fresh medium. The washed cells were then co-cultured with cDC1 for 24 h, followed by the addition of 100,000 CTV (Thermofisher, #C34557) labeled CD25-negative OT-I T cells to each well. Three days post co-culture, cells were collected and analyzed by flow cytometry to evaluate DC markers, T cell proliferation and T cell markers.

Treatment of human GBM patient-derived organoids with oHSV1

Fresh human GBM tumor tissues were processed following surgical resection from patients at The Second Affiliated Hospital, Zhejiang University School of Medicine, with appropriate consent and following an IRB-approved protocol (IR2022453). A total of two patient-derived samples were collected in this experiment. Initially, the fresh tumor tissues were finely minced into small pieces approximately 0.5–1 mm in diameter using fine dissection scissors. These mince fragments were then subjected to washing with sterile PBS to eliminate any cellular debris. Subsequently, the tumor pieces were incubated in RBC lysis buffer (Leagene, #CS0001) at room temperature for 5 min and washed again with sterile PBS. The minced tumor pieces were subsequently cultured in Costar 6-well Clear Flat Bottom Ultra-Low Attachment plates (Corning, #3471) supplemented with DMEM/F12 (Gibco, #11330-032) supplemented with B-27 (Gibco, #12587-010), 20 ng/mL recombinant human EGF protein (R&D, #236-EG), 20 ng/mL recombinant human FGF basic protein (R&D, #4114-TC), 1% penicillin/streptomycin (Biosharp, #P1400), 1% sodium pyruvate (Gibco, #11360-070), and 1% GlutaMax supplement (Gibco, #35050-061). These cultures were maintained on an orbital shaker (Thermo Fisher Scientific) rotating at 120 rpm within a sterile incubator at 37°C with 5% CO_2 and 90% humidity. For the organoid killing assay, a single organoid (0.5–1 mm) was seeded into each well of a 24-well plate that had been pretreated with IBRD9 (Selleck, #S7835, 2 μM) for 24 h. After pretreatment, the organoids were treated with 2×10^4 PFU oHSV1 for 6 h. Following the viral treatment, the culture medium was replaced. After an additional 24–36 h, the assays of the organoids were assessed according to the manufacturer's protocol.

Treatment of human GBM patient-derived sections with oHSV1

Fresh human GBM tumor tissues were processed following surgical resection from patients at The Second Affiliated Hospital, Zhejiang University School of Medicine, with appropriate consent and following an IRB-approved protocol (IR2022453). A total of two patient-derived samples were collected in this experiment. Briefly, tumor slices were prepared from normal brain tissue and tumor-adjacent tissues. Subsequently, the tumor tissues were placed in ice-cold sucrose-ACSF buffer with the following composition: 280 mM sucrose, 5 mM KCl, 2 mM $MgCl_2$, 1 mM $CaCl_2$, 20 mM glucose, 10 mM HEPES, 5 mM Na^+-ascorbate, 3 mM thiourea, 2 mM NaCl, and 29 mM pyruvate; all adjusted to a pH of 7.3. The tissue was then sliced into 250-350 μm-thick sections using a VT1200S VibraTome (Leica). The tumor sections were cultured in a Costar 6-well Clear Flat Bottom Ultra-Low Attachment plate (Corning, #3471) with DMEM/F12 (Gibco, #11330-032) supplemented with B-27 (Gibco, #12587-010), 20 ng/mL recombinant human EGF protein (R&D, #236-EG), 20 ng/mL recombinant human FGF basic protein (R&D, #4114-TC), 1% penicillin/streptomycin (Biosharp, #P1400), 1% sodium pyruvate (Gibco, #11360-070), and 1% GlutaMax (Gibco, #35050-061). The plate was then placed on an orbital shaker (Thermo Fisher Scientific) and rotated at 120 rpm within a sterile incubator set at 37°C, 5% CO_2, and 90% humidity. For the virus replication assay, one section was removed and transferred to a pretreated 6-well plate (Corning, #3471). The section was pretreated with IBRD9 (Selleck, #S7835, 2 μM) for 24 h and then treated with 2×10^4 PFU oHSV1 for 6 h, after which the culture medium was replaced. After 24–36 h, the sections were collected for quantitative real-time PCR (qRT−PCR) analysis to measure oHSV1 replication, and immunohistochemical staining was performed to detect oHSV1.

QUANTIFICATION AND STATISTICAL ANALYSIS

Statistical analysis

Statistical analyses were performed using GraphPad Prism (v8.4.3) and R (v4.0.3). The Unpaired two-sided Student's t test was used to calculate significance unless stated otherwise. When more than two groups were assessed, data were assessed by one-way ANOVA and two-way ANOVA. Survival comparison was performed using the log rank test. Significance was assumed to be reached at $p < 0.05$. In all graphs, $^*p < 0.05$, $^{**}p < 0.01$, $^{***}p < 0.001$, $^{****}p < 0.0001$, NS, not significant. Details of all statistical tests used can be provided in the respective figure legends.

Software

R (v4.0.3), Graphpad Prism (v8.4.3) and FlowJo (v10.4) were utilized in this study.